Deciphering the scopolamine challenge rat model by preclinical functional MRI

Gergely Somogyi[1#], Dávid Hlatky[1#], Tamás Spisák[1, 2], Zsófia Spisák [1], Gabriella Nyitrai[1], András Czurkó[1*]

[#] These authors contributed equally to this work.

[1] Preclinical Imaging Center, Pharmacology and Drug Safety Research, Gedeon Richter Plc., Budapest, Hungary

[2] Department of Diagnostic and Interventional Radiology and Neuroradiology, University Hospital Essen, Essen, Germany

[*]Corresponding author:

András Czurkó

Pharmacology and Drug Safety Research

Gedeon Richter Plc.,

POB: 27, Budapest 10, H-1475,

Hungary.

Tel.: +36 1 431 5870;

fax: +36 1 505 7275.

E-mail address: czurkoa@richter.hu

This PDF file includes:

Main Text

Figures 1 to 4

Tables 1

Abstract

During preclinical drug testing, the systemic administration scopolamine (SCO), a cholinergic antagonist, is widely used. However, it has limited predictive validity partly due to its peripheral side-effects. Therefore, objective neuroimaging measures would enhance its translational value. To this end, in Wistar rats, we measured whisker-stimulation induced functional MRI activation after SCO, peripherally acting butylscopolamine (BSCO), or saline administration. Besides the commonly used gradient-echo echo-planar imaging (GE EPI), we also used an arterial spin labeling method in isoflurane anesthesia. With the GE EPI measurement, SCO decreased the evoked BOLD response in the barrel cortex (BC), while BSCO increased it in the anterior cingulate cortex. In a second experiment, we used GE EPI and spin-echo (SE) EPI sequences in a combined (isoflurane + i.p. dexmedetomidine) anesthesia to account for anesthesia-effects. Here, we also examined the effect of donepezil. In the combined anesthesia, with the GE EPI, SCO decreased the activation in the BC and the inferior colliculus (IC). BSCO reduced the response merely in the IC. Our results revealed that SCO attenuated the evoked BOLD activation in the BC as a probable central effect in both experiments. The likely peripheral vascular actions of SCO with the given fMRI sequences depended on the type of anesthesia or its dose.

Significance Statement

Rodent functional MRI (fMRI) is a powerful and promising tool for translational research, as it bridges the gap between animal experiments and human neuroimaging. Scopolamine (SCO) is a standard reference drug for inducing experimental cognitive impairment in both animals and humans, however, it has limited predictive validity partly due to its peripheral side-effects. We measured whisker-stimulation induced fMRI activation after injecting SCO or its peripherally acting analog with different fMRI sequences in two different anesthesia type and analyzed the data with different

statistical inferences. We deciphered that the likely peripheral vascular actions of SCO with the given fMRI sequences depended on the type of anesthesia or its dose.

Introduction

On the bases of the cholinergic hypothesis of geriatric memory dysfunction (1) scopolamine became a standard reference drug for inducing experimental cognitive impairment in both animals and humans (2-4). The so-called "scopolamine challenge" is widely used in preclinical testing of new substances for putative procognitive compounds (5-7). This approach, i.e. the reversal of scopolamine-induced impairments, however, has limited predictive validity as it tends to yield a high number of false positives (8, 9). Specifically, one of the important limitations of the scopolamine (SCO) model is its peripheral side-effects that can influence the learning and memory deficits observed at higher doses of SCO (4). In fact, part of the early controversy in using the SCO model was based on the apparent "amnestic" actions of SCO methybromide - a quaternary amine analog of SCO that does not readily enter the brain (10-13).

Just the opposite way, by emphasizing the peripheral vascular action of SCO as a primary mechanism, a SCO provocation-based pharmaco-MRI model was proposed as a test for procognitive agents (5, 14). In this case, another non-blood-brain barrier-penetrating anticholinergic drug, butylscopolamine (BSCO) was used. Indeed, in a pharmaco-MRI study, negative blood-oxygen-level-dependent (BOLD) changes in the prefrontal cortex in isoflurane anesthesia were induced by the i.v. injection of both SCO and BSCO (14). However, in α-chloralose anesthesia in a similar preclinical pharmaco-MRI study, increased BOLD contrast in the frontal (orbital) cortex and olfactory nuclei were found after the i.v. injection of SCO while it was absent after BSCO (15). These diverging results highlight the difficulty of interpreting preclinical

pharmaco-MRI data (16) complicated by the use of different anesthetic regimes (17) that can introduce potential confounds (18).

As MRI acquisition parameters could influence the different signal components of BOLD (19), contrasting gradient-echo (GE), spin-echo (SE) echo-planar imaging (EPI) and functional arterial spin labeling (ASL) could address interpretation issues and provide a deeper insight into the SCO model. Likewise, performing functional MRI measurements in a block-design in different anesthetic regimes could yield useful, translatable information for the SCO challenge in preclinical drug testing efforts.

Therefore, in the present study, we measured whisker stimulation-induced BOLD activation and the effect of SCO in two experiments on an ultrahigh field (9.4 T) preclinical MRI system in rats. In the first experiment, SCO and peripherally acting analogue BSCO were used as a pretreatment and BOLD activation were measured to air-puff stimulation of the whisker pad with GE echo-planar imaging (EPI) sequence and with functional ASL in isoflurane anesthesia.

In the second experiment, SCO and BSCO were used in the same way in combined i.p. medetomidine + isoflurane anesthesia and additionally the effect of cholinesterase inhibitor donepezil (DON) was examined on the whisker stimulation evoked BOLD response with both GE EPI and SE EPI sequences.

Results

For weights, average in-scanner motions, isoflurane doses and respiration rates see Supplementary Materials and Methods (Table S1, S2). These data show that neither of these variables had any effect related to the applied treatment in either experiment.

The whisker stimulation evoked BOLD activation was variable in size and depended on the anesthesia and MRI sequences but the barrel cortex (BC) was always involved. Overview of the experiments is shown in Fig. 1 and Table S3.

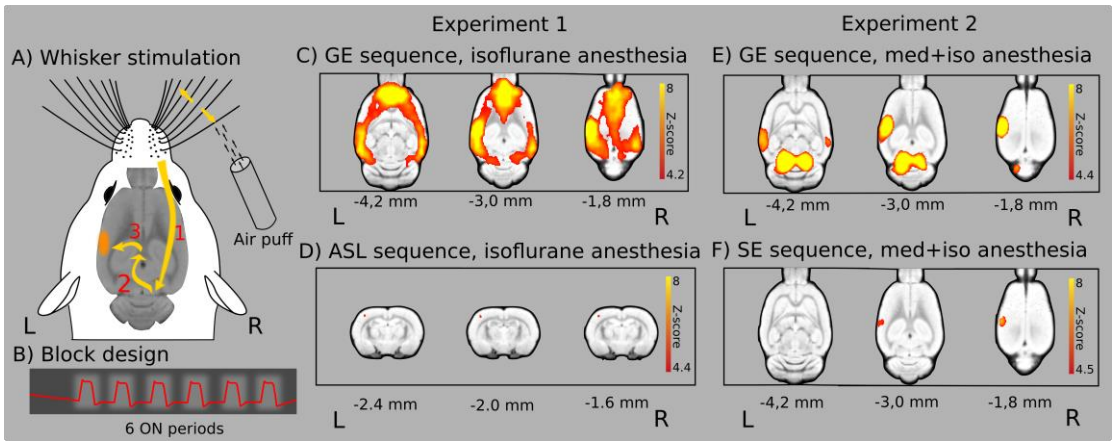

Fig. 1. Air-puff stimulation of the right whisker pad in experiment 1 and 2. *(A)* Signal path from whisker stimulation to activation in the barrel cortex ((1) trigeminal nerve, brain stem, (2) sensory information to the thalamus, (3) the primary somatosensory barrel cortex (BC)). *(B)* Block-design of whisker air-puff stimulation. *(C)* Widespread cortical BOLD activation in isoflurane anesthesia with gradient-echo (GE) EPI sequence. *(D)* Limited activation detected in the BC with the ASL sequence in the same experiment. *(E)* Pronounced activation in the left BC and bilaterally in the IC in the combined anesthesia. *(F)* Limited activation in the BC with the SE sequence in the same experiment. The Z-scores represent voxelwise statistical inference ($p<0.05$ correcting for multiple comparisons via GRF theory based FWER). The corresponding colorbars are depicted on the right. The z (or y) coordinates (distance from Bregma) are given below the slices (L and R stand for directions).

Whisker stimulation evoked BOLD responses in isoflurane anesthesia with gradient-echo (GE) EPI sequence

In experiment 1, air-puff stimulation of the right whisker pad evoked widespread cortical BOLD activation in all three treatment groups (Fig. 1, Fig. S1 and Table S3). In the saline (Sal) group, the strongest activation peak was found in the left primary somatosensory cortex, barrel field (L S1 BF). The activation extended bilaterally to wide cortical areas, rostrally it involved the orbital, infralimbic, prelimbic and cingulate cortices, and caudally the auditory, posterior parietal, visual, perirhinal and retrosplenial cortices. For the SCO and BSCO group activations see Fig. S1 and Table S3. For the analysis with three different statistical inferences (voxel, cluster, pTFCE) see Table S4. For local maxima and signal changes with voxelwise statistical inference see Table S5.

Treatment group differences in isoflurane anesthesia with GE EPI sequence

Between-group fMRI contrasts revealed statistically significant differences in the groupwise activation patterns between the treatment groups (Fig. 2, Table S6). The Sal > SCO contrast with voxelwise statistics (Fig. 2a, Table S6) revealed three small areas of statistically significant decreased BOLD response. The two larger blobs were in the L S1 BF and in the left primary visual cortex, monocular area (L V1 M). With clusterwise statistics, an additional larger blob in the right primary somatosensory cortex, forelimb region (R S1 FL) was found (Fig. 2a, Table S6). With pTFCE (GRF corrected (4.7 < z)) statistics, three additional blobs were significant besides the L V1 M, the secondary somatosensory cortex (R S2), the presubiculum (L PrS) and the primary auditory cortex (R Au1, Fig. 2a, Table S6).

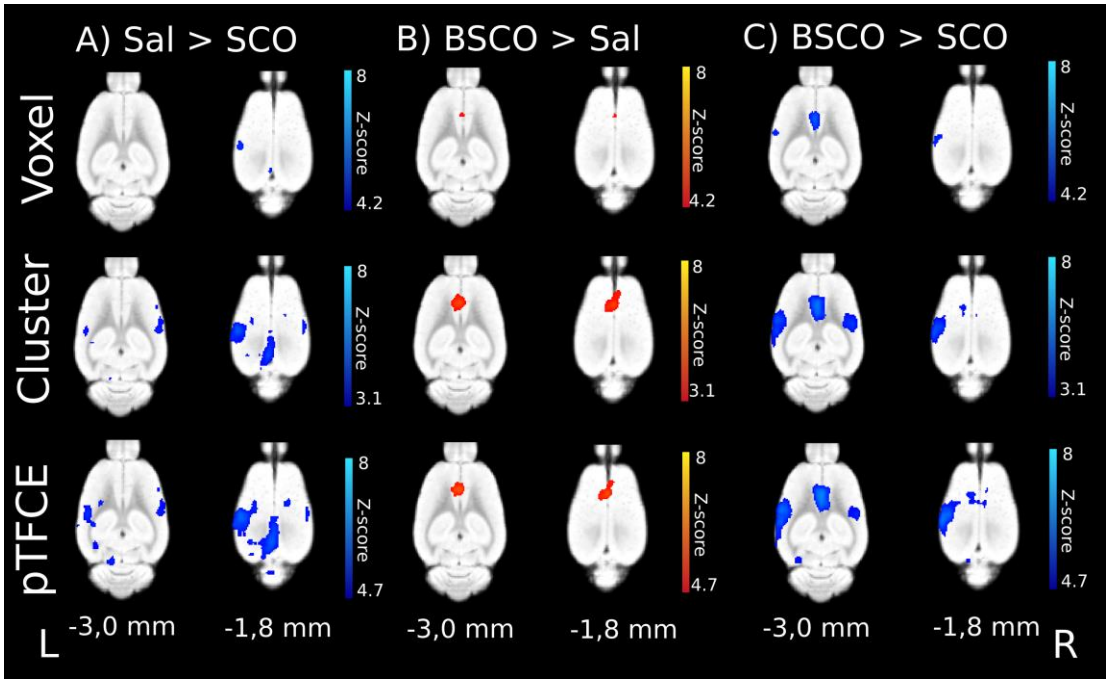

Fig. 2 Evoked BOLD response differences between groups with GE EPI sequence in isoflurane anesthesia. *(A)* Decreased BOLD response in the scopolamine (SCO) treated group compared to saline (Sal > SCO). *(B)* Increased BOLD response in the butylscopolamine (BSCO) group compared to saline (BSCO > Sal). *(C)* Differences between the SCO and BSCO treated groups (BSCO > SCO). The Z-scores in the upper row (Voxel) represent voxelwise statistical inference ($p<0.05$ correcting for multiple comparisons via GRF theory based FWER, navy blue-to-light blue or red-to-yellow from $z=4.2$ to $z=8$); in the middle row (Cluster) clusterwise statistical inference ($p<0.05$ correcting for multiple comparisons via GRF theory based FWER and a cluster forming threshold of $p=0.001$, navy blue-to-light blue or red-to-yellow $z=3.1$ to $z=8$); in the lower row probabilistic TFCE (pTFCE) statistics ($p<0.05$ correcting for multiple comparisons via GRF theory based FWER, navy blue-to-light blue or red-to-yellow $z=4.7$ to $z=8$) from the same data. The corresponding colorbars are depicted on the right. The z coordinates (distance from Bregma) of the selected slices (-3.0 mm; -1.8 mm) are given at the bottom of the figure (L, R stands for directions).

In the SCO > Sal contrast only the uncorrected pTFCE ($3.1 < z$) statistics revealed a difference in the cingulate cortex (L Cg1, Table S6). In the BSCO > Sal contrast all statistics (Fig. 2b, Table S6) revealed significant difference in the cingulate cortex (L Cg2 or Cg1, Table S6).

In the BSCO > SCO contrast (Fig. 2c, Table S6) the combination of the Sal > SCO (Fig. 2a, Table S6) and BSCO > Sal (Fig. 2b, Table S6) contrasts appeared. Voxel level statistics revealed differences in the L S1 BF and L Cg2. Cluster level statistics

additionally revealed the R S1 BF and the pTFCE (GRF corrected (4.7 < z) revealed three additional ones.

In the Sal > BSCO and SCO > BSCO contrasts there were no significant differences with clusterwise statistics. For the voxelwise and pTFCE statistics see Supplementary Table (Table S6).

Whisker stimulation evoked responses with functional ASL sequence in isoflurane anesthesia

Whisker stimulation-induced activations were focal with the ASL sequence. The combined effect of Sal, SCO and BSCO induced small, focal activations in the L S1 BC and in the L ECIC (Fig. S2) with clusterwise statistical inference. In the L BC significant blobs appeared in the Sal (as shown also in Fig. 1) and BSCO treatment groups (this effect was visible with the voxelwise and GRF corrected pTFCE statistic as well), but in SCO this focal activation could only be detected by the uncorrected pTFCE (3.1 < z) inference. These statistical results are explicable with the signal changes in the masked L S1 BF as shown in Fig. S2. The uncorrected pTFCE (3.1 < z) statistics detected the L S1 BF in the SCO group (Fig. S3 and Tables S7), but there were additional smaller activations in the left inferior colliculus and retrosplenial cortex (Tables S7). Between-group fMRI analysis of the groupwise activation patterns revealed no statistically significant differences between the treatment groups. For the effect of the treatment groups on signal changes during functional ASL measurements and the difference between the tagged and non-tagged ASL images over time see Supplementary Fig. S4 and Fig. S5.

Whisker stimulation evoked BOLD responses in medetomidine-isoflurane combined anesthesia with the GE EPI sequence

In experiment 2, the whisker stimulation-induced BOLD activations had a characteristic focal appearance (Fig. 1) in all four treatment groups (Fig. S6 and Tables S8). In the Sal group, with voxelwise statistical inference, the strongest activation peaked in the left external cortex of inferior colliculus (L ECIC) but the large activation

area bilaterally involved the inferior colliculus (IC) and extended rostrally, bilaterally to the medial geniculate nucleus and on the left, to the ventral posteromedial thalamic nucleus (VPM). A second large activation area peaked in the L S1 BF that also extended to the left auditory cortex and temporal association cortex. The third smaller activation area peaked in the right primary auditory cortex (R Au1).

In the SCO and BSCO groups (1.0 mg/kg) the whisker stimulation-induced activation patterns were very similar to the Sal group (Fig. S6 and Tables S8). In the DON group, the same activation pattern was seen but the activations were somewhat smaller (Fig. S6 and Tables S8).

Treatment group differences in medetomidine-isoflurane combined anesthesia with the GE EPI sequence

Between-group fMRI analysis contrasts revealed significant differences in this measurement (Fig. 3, Table 1). In the Sal > SCO contrast the voxelwise statistical inference revealed decreased activation due to SCO in the L ECIC and the L S1 BF while clusterwise statistics highlighted only the L ECIC (Table S9). The pTFCE statistics (GRF corrected (4.7 < z)), detected the L ECIC and one voxel in the L S1 BF while the uncorrected pTFCE (3.1 < z) statistics detected a larger blob in the L S1 BF and the left and right ECIC (L & R ECIC, Table 1).

In the Sal > BSCO contrast, voxelwise and pTFCE (GRF corrected (4.7 < z)) statistics revealed a statistically significant decreased BOLD response due to BSCO in the L ECIC (Table 1 and Table S9).

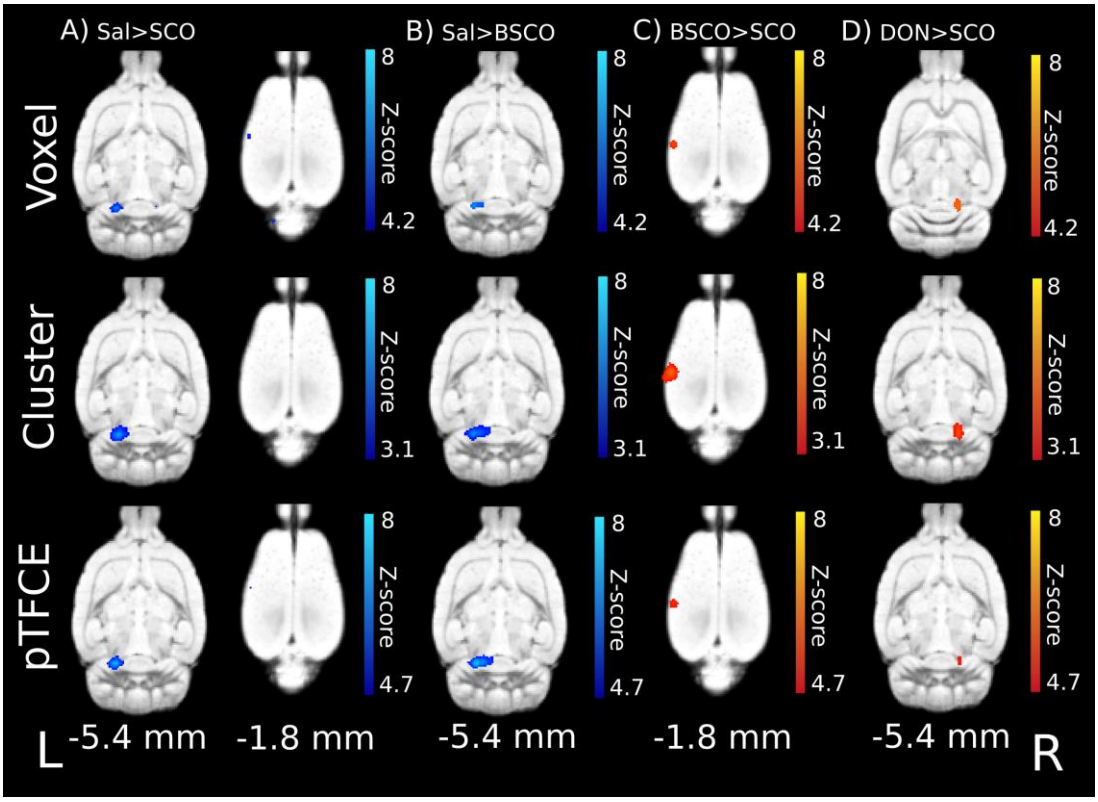

Fig. 3 Evoked BOLD response differences between groups with GE EPI sequence in medetomidine-isoflurane combined anesthesia. *(A)* Sal > SCO, *(B)* Sal > BSCO, *(C)* BSCO > SCO and *(D)* DON > SCO contrast. Decreased BOLD responses in the BC due to SCO *(A*, *C)* and in the IC due to both SCO and BSCO *(A*, *B)*. Increased BOLD responses in the right IC in the DON treatment group compared to the SCO group *(D)*. The Z-scores in the upper row (Voxel) represent voxelwise statistical inference ($p<0.05$ correcting for multiple comparisons via GRF theory based FWER, navy blue-to-light blue or red-to-yellow from z=4.2 to z=8); in the middle row (Cluster) clusterwise statistical inference ($p<0.05$ correcting for multiple comparisons via GRF theory based FWER and a cluster forming threshold of p=0.001, navy blue-to-light blue or red-to-yellow z=3.1 to z=8); in the lower row probabilistic TFCE (pTFCE) statistics ($p<0.05$ correcting for multiple comparisons via GRF theory based FWER, navy blue-to-light blue or red-to-yellow z=4.7 to z=8) from the same data. The corresponding colorbars are depicted on the right. The z coordinates (distance from Bregma) of the selected slices (-5.4 mm; -1.8 mm) are given at the bottom of the figure (L, R stands for directions).

In the BSCO > SCO contrast all statistics revealed a difference in the L S1 BF (Fig. 3, Table 1 and Table S9). Likewise comparing the Sal > SCO and Sal > BSCO contrasts, it

might suggest that in this measurement changes in the L ECIC could be a peripheral effect (Fig. 3, 4 and Table 1).

In both the DON > SCO and DON > BSCO contrasts there were significant differences in the R ECIC area with all statistics (Fig. 3, 4 and Table 1 and Table S9).

In the SCO > Sal, SCO > BSCO, SCO > DON and BSCO > Sal contrasts only the uncorrected pTFCE (3.1 < z) statistics found differences (Table 1 and Table S9).

In the BSCO > DON and DON > Sal contrasts there were no differences with either statistics (Table S9).

Whisker stimulation evoked BOLD responses in medetomidine-isoflurane combined anesthesia with SE EPI sequence

In this measurement the whisker stimulation-induced BOLD activations were focal and localized to the L S1 BF in all four treatment groups (Fig. S7 and Table S10).

Treatment group differences in medetomidine-isoflurane combined anesthesia with the SE EPI sequence

Between-group fMRI contrasts revealed significant activation differences only with pTFCE statistics in this measurement, (Table 1). In the BSCO > SCO contrast, with the pTFCE (GRF corrected (4.7 < z)) statistics only one voxel difference was found in the L S1 BF. This one voxel difference also mirrored in the L S1 BF in the DON > SCO and DON > BSCO contrasts (Table 1). The uncorrected pTFCE (3.1 < z) also revealed these and other differences in most contrasts (Table 1 and Table S9).

Table 1. Evoked activation differences in medetomidine-isoflurane combined anesthesia with GE EPI and SE EPI sequences (the size of blobs in mm^3 and the brain structures to which Z-score [pTFCE statistical inference, p=0.05 via GRF theory base FWER] peaks belong to). p. a. - stands for probable artefact, as our gradient echo images are not accurate enough around the cerebellum to firmly conclude the difference.

Exp. 2				
Treatment group	*EPI sequence*	*Size of pTFCE-wise blobs (mm^3)*		*Structures to which pTFCE-wise Z-score peak belongs to:*
		Uncorrected (3.1<z)	*Corrected (4.7<z)*	
Sal > SCO.	*GE*	14.2	7.3	L ECIC - Left external cx inferior colliculus
		5.1	-	R ECIC -Right external cx inferior colliculus
		4.0	0.01	L S1 BF - Left primary somatosensory cortex, barrel field
		0.1	-	Left cerebellar lobe (p.a.)
	SE	0.02	-	L S1 BF - Left primary somatosensory cortex, barrel field
Sal > BSCO	*GE*	33.6	13.3	L ECIC - Left external cortex inferior colliculus
	SE	-	-	-
Sal > DON	*GE*	20.8	-	Left cerebellar lobe (inferior colliculus)
	SE	-	-	-
SCO > Sal	*GE*	4.0	0.2	Left cerebellar lobe
		0.3	-	Right cerebellar lobe (p.a.)
		0.2	-	Right cerebellar lobe (p.a.)
	SE	0.3	-	L S1 J primary somatosensory cortex, jaw region
		0.3	-	VPM –ventral posteromed thalamic nucleus
SCO > BSCO	*GE*	0.8	-	L cerebellar lobes (p.a.)
	SE	-	-	-
SCO > DON	*GE*	3.1	-	Right cerebellar lobes -Crus2
		0.2	-	Left Cerebellar lobes (p.a.)
		0.1	-	L VTg – Left ventral tegmental nucleus
	SE	0.2	-	R PrS - Right presubiculum
BSCO > SCO	*GE*	5.9	0.5	L S1 BF – Left primary somatosensory cortex, barrel field
	SE	0.02	0.01	L S1 BF – Left primary somatosensory cortex, barrel field
BSCO > Sal	*GE*	5.2	-	L Cerebellar lobe
	SE		-	
DON > SAL	*GE*	-	-	-
	SE	1.1	-	L S1ULp – Left primary somatosensory cortex, upper lip
		0.1	-	L S1 BF – Left primary somatosensory cortex, barrel field
DON > SCO	*GE*	6.8	1.8	R ECIC – Right external cx inferior colliculus
	SE	2.2	0.01	L S1 BF primary somatosensory cortex, barrel field
DON > BSCO	*GE*	7.0	1.8	R ECIC - Right external cortex of inferior colliculus)
		2.1	-	Right cerebellar lobes (p.a.)
	SE	0.1	0.01	L S1 BF – Left primary somatosensory cortex, barrel field

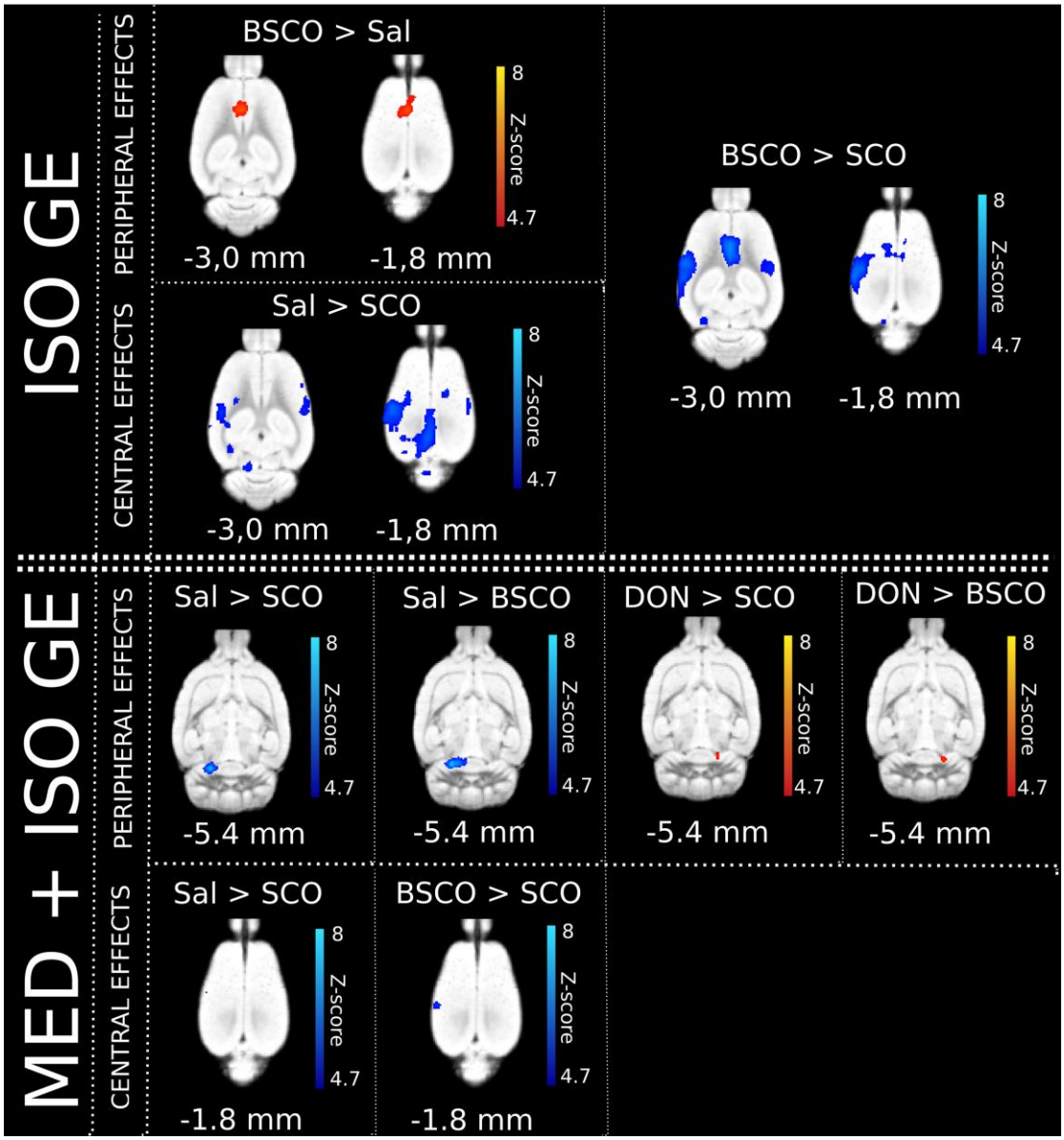

Fig. 4 Summary figure of the whisker-stimulated evoked BOLD response differences between groups with GE EPI sequences in both anesthesia types (isoflurane – top: ISO GE; medetomidine-isoflurane – bottom: MED + ISO GE) according to their peripheral/central effects. In ISO anesthesia, in the BSCO > Sal contrast a peripheral effect, in the Sal > SCO contrast probable central effects are seen. In the BSCO > SCO contrast both effects are seen. In the combined anesthesia (MED + ISO GE) we found probable peripheral effects at the (right or left) inferior colliculus / transverse sinuses in the Sal > SCO, Sal > BSCO, DON > SCO and DON > BSCO contrasts. The central effects (in the left barrel field) are shown in the BSCO > SCO and Sal > SCO group differences. The Z-scores represent the probabilistic TFCE (pTFCE) statistics ($p<0.05$ correcting for multiple comparisons via GRF theory based FWER, navy blue-to-light blue or red-to-yellow $z=4.7$ to $z=8$). The corresponding colorbars are depicted next to every group

difference on the right. The z coordinates (distance from Bregma) of the selected slices (-5.4 mm; -1.8 mm) are given at the bottom of the figure.

Time course of the relative BOLD activation in the different groups

The time courses of relative BOLD activation due to the six whisker stimulation blocks in the average activated barrel field (where according to the type of measurement the merged activations were Z-score > 12, voxelwise) were calculated. In all EPI measurements, the activations were visible during the stimulation blocks. The type of anesthesia and the size of the activated barrel field influenced the relative amplitudes of the BOLD activations (Fig. S8). The relative BOLD change also averaged into one block according to the different pretreatments (Fig. S9).

Discussion

Acute administration of SCO, in several human fMRI studies, induced decreased regional CBF or attenuation in the memory-task-induced increases of regional CBF and BOLD activation in various frontal brain areas using memory and attentional paradigms (20-24). These data resemble the SCO-induced hypofrontality in humans (25) and rats (14) induced by the acute i.v. injection of SCO. The acute i.v. infusion of SCO, however, could transiently produce a reduction of the heart rate and blood pressure (26) and this could interfere with the neuroimaging data described above (27).

In our neuroimaging study, to avoid the transient effects of SCO, we did not use the traditional preclinical pharmaco-MRI approach with acute i.v. anticholinergic infusion but a “task” fMRI with a pretreatment (1 hour). This pretreatment is similar to those behavioural studies where SCO is used to induce cognitive impairment (11). We used the preclinical MRI as a “task” fMRI, by measuring the whisker stimulation-induced

BOLD activation in a block design. With this approach, we could not see the dramatic reduction of perfusion or negative BOLD in the prefrontal cortex (5, 14, 25).

Originally many years before, when we started to investigate the effect of SCO, we surprisingly observed increased BOLD activation in widespread frontal cortical areas due to both SCO and BSCO as a pretreatment (in 1 mg/kg dose; in isoflurane anesthesia) during the whisker stimulation (See Fig. S10, Spisák et al. unpublished data). Similarly, in a previous perfusion imaging study with similar SCO pretreatment (1 hour) an increased rCBV was found in young dogs, unexpectedly (28). Furthermore, in the frontal and prefrontal cortical areas during a working memory task hyperactivation due to SCO was also reported (29).

One of the limitations of the SCO model is its peripheral side-effects that can influence the learning and memory deficits at higher doses of SCO (4). In a preclinical pharmaco-MRI study the 1 mg/kg SCO and BSCO performed similarly in isoflurane anesthesia (14), while in α-chloralose anesthesia the 0.8 mg/kg SCO increased the BOLD contrast in the frontal cortex but the same dose of BSCO not (15). Importantly, in an eminent translational study of the SCO model, 0.3 mg/kg dose of SCO was used, in rats (6). Therefore, in our first experiment, 0.3 mg/kg dose of SCO and BSCO were used, as a pretreatment.

In experiment 1 (Exp. 1), in isoflurane anesthesia with GE EPI sequence, the whisker stimulation evoked a widespread cortical BOLD activation and group differences revealed a decreased BOLD response in the barrel cortex (BC) due to SCO but not due to BSCO. This SCO result is in line with the human fMRI studies where the SCO typically attenuated the evoked BOLD activation. Interestingly, BSCO increased the evoked BOLD response in the anterior cingulate cortex (Cg1). Only the uncorrected pTFCE statistics detected this effect in case of the SCO pretreatment. This result would mark a peripheral effect on the BOLD activation by BSCO that separated from those of SCO at the 0.3 mg/kg dose, in isoflurane anesthesia.

In Exp. 1, in the ASL-BOLD measurement the whisker stimulation of the combined effect of Sal, SCO and BSCO induced small, focal activations in the L BC and the L ECIC

(Fig. S2) with clusterwise statistical inference. In the L BC significant blobs appeared in the Sal and BSCO treatment groups, but in SCO this focal activation could only be detected by the uncorrected pTFCE (3.1 < z) inference (30). The apparent difference in activation maps between the GE EPI and ASL sequences may be due to the differences in their signal to noise ratio. Noteworthy, that the GE EPI sequence is also more sensitive to the intra- and extravascular effects of BOLD consequently for the larger pial surface veins that are probably sensitive to the peripheral effects of drugs. Exp. 1 was in isoflurane anesthesia that is ideal for non-invasive longitudinal studies (31-35). Although isoflurane lacks functional groups and only interacts with its targets through weak polarization forces (36, 37), there is a chance that it could interfere with the cholinergic system (38, 39). Isoflurane may also weaken the blood-brain barrier (40) by modulating tight junction protein expression (41), that may influence the effect of BSCO in our study.

Furthermore, isoflurane anesthesia dilates blood vessels (42, 43), and may induce propagating slow calcium waves reflected in pan-cortical BOLD fMRI activation (44). These may explain the widespread cortical BOLD activation evoked by the whisker stimulation with GE EPI sequence in isoflurane anesthesia in Exp. 1. To address some of the above issues, in Exp. 2 we used combined medetomidine-isoflurane anesthesia, and higher doses of our drug pretreatments as medetomidine can constrict both pial arteries and veins (42). Here the same whisker stimulation, with the GE EPI sequence, evoked a characteristic focal BOLD activation. It involved both the left BC and bilaterally the central nuclei of the inferior colliculus (IC). This profound bilateral activation of the IC is an unexpected finding, although the strong background acoustic noise of the scanner is always present. Our fMRI measurement used whisker stimulation in a block design. Therefore, it may look surprising that a constant, background acoustic noise would induce profound activation. It was demonstrated, on the other hand, that the scanner acoustic noise can modulate the somatosensory stimulation. Specifically, the simultaneous acoustic noise facilitated the activation of the somatosensory cortex (45). The IC receives ascending projections from both

auditory and somatosensory nuclei. Therefore it should be regarded, as a node in multisensory integration (46, 47). Nonetheless, the profound activation of the IC in the combined medetomidine-isoflurane anesthesia in Exp 2 is still remarkable. Regarding anesthesia, it is also interesting that a PET study of auditory activation also observed significantly higher 18F-FDG uptake in the IC in combined medetomidine anesthesia compared to another type of anesthesia (48).

Group differences with the GE EPI sequence show that both SCO and BSCO decreased the BOLD activation in the IC (Sal > SCO, Sal > BSCO), while SCO also decreased the BOLD activation in the BC. In the BSCO > SCO contrast all statistics revealed the difference in the L S1 BF. These results may suggest that SCO could decrease the BOLD activation in the L S1 BF as through a central effect. Likewise comparing the Sal > SCO and Sal > BSCO contrasts, it might suggest that in this anesthesia the bilaterally decreased activation in the ECIC could be at least partially a peripheral effect that could involve the left and right transverse sinuses. A similar mechanism could explain the decrease in activation in the L ECIC in the Sal > DON contrast, although it localized to the left, activated side. This unilateral effect of DON on the left side can explain the unilateral R ECIC effect in both the DON > SCO and DON > BSCO contrasts.

Therefore, we think that in this anesthesia, we observed both the central (BC) and the peripheral (IC) effects of SCO. With the same GE EPI sequence, we could not reveal a significant difference in the BC, in the DON > SCO contrast. Interestingly, differences in some voxels were detected in the SE EPI measurement by the pTFCE statistical inference.

Our study attempted to preclinically decipher the neuroimaging correlates of the SCO challenge with different statistical inferences. We revealed that the SCO attenuated the evoked somatosensory BOLD activation in the BC, independently from the anesthesia. Its perceived peripheral action depended on the type of anesthesia, dose and fMRI sequences.

Materials and methods

Animals

Thirty-four drug-naïve adult male Wistar (RJ Han, Harlan Laboratories (Envigo)) rats were used for the two experiments (Exp.1: *n*=18; Exp.2: *n*=16,). The animals were kept by controlled laboratory conditions (constant temperature and humidity) in polycarbonate cages under standard in a 12h light/dark cycle with the light on at 6:00 a.m. The rats were fed with conventional laboratory rat food (sniff R/M + H Spezieldiäten GmbH D-59494 Soest), with food and water ad libitum. All the procedures conformed to the guidelines of the National Institutes of Health for the care and use of laboratory animals and were approved by the local Ethical Committee of Gedeon Richter Plc. and were carried out in strict compliance with the European Directive 2010/63/EU regarding the care and use of laboratory animals for experimental procedures. All efforts were made to minimize the number of animals as well as pain or discomfort.

Experimental design and drug treatments

The effect of drug pretreatments on the functional MRI activity was examined in a pseudo-randomized cross-over design such that equal numbers of animals received each drug of the given experiment on any given measurement day. There was a minimum interval of seven days between repeated measurements of the same animal. For the average weight of the animal groups see Supplementary Materials and Methods (Table S1, S2).

In experiment 1 (Exp.1), conscious animals received saline (2 ml/kg) or SCO (scopolamine hydrobromide, Tocris) or BSCO (Scopolamine N-butyl bromide, Sigma Aldrich) as pretreatment 1 hour before the start of the MRI measurement. SCO or BSCO were dissolved in distilled water or saline, respectively, and injected intraperitoneally at a dose of 0.3 mg/kg.

In experiment 2 (Exp.2), conscious animals received saline (2 ml/kg), SCO (1 mg/kg), BSCO (1 mg/kg) or DON (Donepezil hydrochloride, 71078800, L77028F, Gedeon Richter Plc.). DON was dissolved in distilled water and was injected at a dose of 3 mg/kg.

Anesthesia during the fMRI scanning

In Exp.1 after the drug pretreatment animals were anesthetized with 5% isoflurane (Forane, Abbot Laboratories) and then maintained at approximately 1.25% during scanning. Other part of the scanning procedure was identical to the procedures outlined previously (33-35). In Exp.2 the anesthesia was introduced with a bolus of medetomidine injection (0.05 mg/kg i.p. dexdor, dexmedetomidine, Orion Pharma) plus 5% isoflurane in air and the concentration of isoflurane was lowered to 0.25% - 1.5% during scanning with the aim of keeping the respiration rate near 60/min. For mean isoflurane dose of the animal groups see Supplementary Materials and Methods (Table S1, S2).

Image acquisition

The MRI experiments were performed on a 9.4 T Varian (Agilent) Direct Drive MRI system (Varian Medical Systems Inc., Palo Alto, CA). MRI system parameters described in detail previously (33-35), also see Supplementary Materials and Methods.
Anatomical images for the fMRI registration were proton density (PD) weighted gradient-echo multi-slice imaging (GEMS) in horizontal orientation, and/or a T2 weighted fast spin-echo multi-slice imaging (FSEMS) anatomical scans in axial orientation, see Supplementary Materials and Methods.

BOLD fMRI EPI sequences

Echo planar imaging (EPI) sequences were used for the BOLD measurements. Gradient-echo EPI (GE EPI: TR/TE = 1000ms/10ms, FA: 90°) and spin-echo EPI (SE EPI:

TR/TE = 1000ms/40ms, FA: 90°) sequences were used (Supplementary Materials and Methods).

ASL fMRI sequence

For multislice arterial spin labeling (ASL) measurements a flow-sensitive alternating inversion recovery (FAIR-ASL, TR/TE = 3.6s/18ms, matrix: 64×64, slice thickness: 2mm, 9 axial slices) sequence was used as described by Nashrallah et al. in (49), see Supplementary Materials and Methods.

Whisker stimulation

During the functional MRI experiments, whisker stimulation by air puffs was used in a block-design fashion. The stimulation procedure was identical to the procedure outlined previously (33-35). The duration of one stimulation block was 30 s followed by 60 s rest and one measurement session contained 6 blocks in case of the GE-EPI and SE-EPI BOLD fMRI measurements with an initial 120 s resting. For ASL-BOLD fMRI, a 36-72 s on-off cycle was used. See Supplementary Materials and Methods for details.

Data analysis

Throughout the image processing procedure, we intended to follow the conventional human- research practice in fMRI analysis. The analysis was carried out in a multistage process using the image analysis software package, FSL (50) (FMRIB's Software Library, www.fmrib.ox.ac.uk/fsl) and in-house developed software tools. Small-animal imaging specific details of the applied image processing pipeline were described in detail previously (33-35). The present data analysis is detailed in Supplementary Materials and Methods in section Data analysis.

Functional MRI analysis

Data processing for functional images (GE EPI, SE EPI and ASL –see also Supplementary Materials and Methods) were carried out using FSL FEAT to investigate the effects of treatment groups and their differences. Gaussian kernel (for spatial smoothing and

high-pass temporal filtering was applied. After signal prewhitening, the first-level statistical analysis was carried out using the general linear model with local autocorrelation correction (51). The analysis -block design convolved with HRF-modelled each rat's data from each session and included 5 noise-ROI-based CompCor (52) confounder variables. Individual statistical Z-score images for the BOLD regressor-of-interest were obtained (average BOLD response to the stimuli). Using the spatial transformations computed during image coregistration and standardization, Z-score maps resulting from the individual statistical analysis were realigned to the common standard space to achieve spatial correspondence during the higher-level analysis.

Fixed-effect group-level statistical analysis was performed on the obtained z-stats using FSL FEAT for voxelwise inference using Gaussian random field (GRF) theory based maximum height thresholding with a (corrected) significance threshold of P=0.05 (53). This approach is robustly valid, show the mean activation in groups, but often too conservative to find differences between treatment groups because it frequently falling below 5% of family-wise error (FWE) rates (54). Similarly, clusterwise thresholding with a corrected significance threshold of P=0.05 at a cluster-forming threshold of p=0.001 (Z > 3.1) was performed. This thresholding method was used to enhance the detection of large activation clusters unlikely to be random false positives originating from multiple comparisons (55). It gives generally better sensitivity than voxelwise inference for disparity in the evoked responses between groups (56). Furthermore, we applied the probabilistic threshold-free cluster enhancement (pTFCE) (30) with a corrected significance threshold of P=0.05. pTFCE provides a natural adjustment for various signal topologies (thereby enhanced P-values directly, without permutation testing). The method can detect spatially extended but relevant signals of low magnitude, as well as small activations, which remain hidden with the robust, but often too conservative voxelwise statistics. This method was implemented in R software (The R Project for Statistical Computing, https://www.r-project.org).

FUNDING AND DISCLOSURE

The study was supported by Gedeon Richter Plc., the Hungarian National Research, Development and Innovation Office (KMOP-1.1.5-08-2009-0001), and the National Brain Research Program (KTIA_NAP_13-1-2013-0001; 2017-1.2.1-NKP-2017-00002). The authors are employees of Gedeon Richter Plc. or were full-time employees of that firm at the time the research was performed, otherwise, they declare no conflicts of interest.

ACKNOWLEDGEMENT

The authors are grateful for the technical assistance of Pálma Diószegi and Katalin Tóthné Fekete.

AUTHOR CONTRIBUTIONS

G.S., D.H., T.S., Zs.S., G.Ny. and A.Cz. designed the experiments; D.H. performed the data acquisition; G.S., T.S., Zs.S. analysed the data; G.S., D.H., T.S., G.Ny. and A.Cz. interpreted the data for the work. G.S., D.H. and A.Cz. wrote the main manuscript text and G.S. prepared figures. All authors reviewed the manuscript.

REFERENCES

1. Bartus RT, Dean RL, 3rd, Beer B, & Lippa AS (1982) The cholinergic hypothesis of geriatric memory dysfunction. *Science* 217(4558):408-414.
2. Ebert U & Kirch W (1998) Scopolamine model of dementia: electroencephalogram findings and cognitive performance. *Eur J Clin Invest* 28(11):944-949.
3. Flood JF & Cherkin A (1986) Scopolamine effects on memory retention in mice: a model of dementia? *Behav Neural Biol* 45(2):169-184.
4. Klinkenberg I & Blokland A (2010) The validity of scopolamine as a pharmacological model for cognitive impairment: a review of animal behavioral studies. *Neurosci Biobehav Rev* 34(8):1307-1350.
5. Hegedus N*, et al.* (2015) Scopolamine provocation-based pharmacological MRI model for testing procognitive agents. *J Psychopharmacol* 29(4):447-455.
6. Lenz RA*, et al.* (2012) The scopolamine model as a pharmacodynamic marker in early drug development. *Psychopharmacology (Berl)* 220(1):97-107.
7. Snyder PJ, Bednar MM, Cromer JR, & Maruff P (2005) Reversal of scopolamine-induced deficits with a single dose of donepezil, an acetylcholinesterase inhibitor. *Alzheimers Dement* 1(2):126-135.
8. Barak S & Weiner I (2011) Putative cognitive enhancers in preclinical models related to schizophrenia: the search for an elusive target. *Pharmacol Biochem Behav* 99(2):164-189.
9. Sarter M (2006) Preclinical research into cognition enhancers. *Trends Pharmacol Sci* 27(11):602-608.
10. Andrews JS, Grutzner M, & Stephens DN (1992) Effects of cholinergic and non-cholinergic drugs on visual discrimination and delayed visual discrimination performance in rats. *Psychopharmacology (Berl)* 106(4):523-530.
11. Buccafusco JJ (2009) The Revival of Scopolamine Reversal for the Assessment of Cognition-Enhancing Drugs. *Methods of Behavior Analysis in Neuroscience,* Frontiers in Neuroscience, eds nd & Buccafusco JJBoca Raton (FL)).
12. Buxton A, Callan OA, Blatt EJ, Wong EH, & Fontana DJ (1994) Cholinergic agents and delay-dependent performance in the rat. *Pharmacol Biochem Behav* 49(4):1067-1073.
13. Ruotsalainen S, Miettinen R, MacDonald E, Koivisto E, & Sirvio J (2000) Blockade of muscarinic, rather than nicotinic, receptors impairs attention, but does not interact with serotonin depletion. *Psychopharmacology (Berl)* 148(2):111-123.
14. Kocsis P*, et al.* (2014) Vascular action as the primary mechanism of cognitive effects of cholinergic, CNS-acting drugs, a rat phMRI BOLD study. *Journal of cerebral blood flow and metabolism : official journal of the*

International Society of Cerebral Blood Flow and Metabolism 34(6):995-1000.
15. Cash D, *et al.* (2005) Visualizing the effects of scopolamine in the rat brain using functional MRI. *J. Cereb. Blood Flow Metab.* 25(1_suppl):S366-S366.
16. Spain A, *et al.* (2015) Neurovascular and neuroimaging effects of the hallucinogenic serotonin receptor agonist psilocin in the rat brain. *Neuropharmacology* 99:210-220.
17. Haensel JX, Spain A, & Martin C (2015) A systematic review of physiological methods in rodent pharmacological MRI studies. *Psychopharmacology (Berl)* 232(3):489-499.
18. Petrinovic MM, *et al.* (2016) A novel anesthesia regime enables neurofunctional studies and imaging genetics across mouse strains. *Sci Rep* 6:24523.
19. Renvall V, Nangini C, & Hari R (2014) All that glitters is not BOLD: inconsistencies in functional MRI. *Sci Rep* 4:3920.
20. Craig MC, *et al.* (2010) The interactive effect of acute ovarian suppression and the cholinergic system on visuospatial working memory in young women. *Psychoneuroendocrinology* 35(7):987-1000.
21. Craig MC, *et al.* (2009) The interactive effect of the cholinergic system and acute ovarian suppression on the brain: an fMRI study. *Horm Behav* 55(1):41-49.
22. Grasby PM, *et al.* (1995) The effect of the muscarinic antagonist scopolamine on regional cerebral blood flow during the performance of a memory task. *Exp Brain Res* 104(2):337-348.
23. Sperling R, *et al.* (2002) Functional MRI detection of pharmacologically induced memory impairment. *Proceedings of the National Academy of Sciences of the United States of America* 99(1):455-460.
24. Thienel R, *et al.* (2009) Muscarinic antagonist effects on executive control of attention. *Int J Neuropsychopharmacol* 12(10):1307-1317.
25. Prohovnik I, Arnold SE, Smith G, & Lucas LR (1997) Physostigmine reversal of scopolamine-induced hypofrontality. *Journal of cerebral blood flow and metabolism : official journal of the International Society of Cerebral Blood Flow and Metabolism* 17(2):220-228.
26. Drevets WC, Zarate CA, Jr., & Furey ML (2013) Antidepressant effects of the muscarinic cholinergic receptor antagonist scopolamine: a review. *Biol Psychiatry* 73(12):1156-1163.
27. Nagaoka T, *et al.* (2006) Increases in oxygen consumption without cerebral blood volume change during visual stimulation under hypotension condition. *Journal of cerebral blood flow and metabolism : official journal of the International Society of Cerebral Blood Flow and Metabolism* 26(8):1043-1051.
28. Tapp PD, *et al.* (2005) Effects of scopolamine challenge on regional cerebral blood volume. A pharmacological model to validate the use of contrast enhanced magnetic resonance imaging to assess cerebral blood volume in

a canine model of aging. *Prog Neuropsychopharmacol Biol Psychiatry* 29(3):399-406.
29. Voss B, *et al.* (2012) Cholinergic blockade under working memory demands encountered by increased rehearsal strategies: evidence from fMRI in healthy subjects. *Eur Arch Psychiatry Clin Neurosci* 262(4):329-339.
30. Spisak T, *et al.* (2018) Probabilistic TFCE: A generalized combination of cluster size and voxel intensity to increase statistical power. *NeuroImage* 185:12-26.
31. de Celis Alonso B, Sergeyeva M, Brune K, & Hess A (2012) Lateralization of responses to vibrissal stimulation: connectivity and information integration in the rat sensory-motor cortex assessed with fMRI. *NeuroImage* 62(3):2101-2109.
32. Masamoto K, Kim T, Fukuda M, Wang P, & Kim SG (2007) Relationship between neural, vascular, and BOLD signals in isoflurane-anesthetized rat somatosensory cortex. *Cereb Cortex* 17(4):942-950.
33. Nyitrai G, *et al.* (2018) Stepwise occlusion of the carotid arteries of the rat: MRI assessment of the effect of donepezil and hypoperfusion-induced brain atrophy and white matter microstructural changes. *PloS one* 13(5):e0198265.
34. Spisak T, *et al.* (2017) Central sensitization-related changes of effective and functional connectivity in the rat inflammatory trigeminal pain model. *Neuroscience* 344:133-147.
35. Spisak T, *et al.* (2019) Purkinje cell number-correlated cerebrocerebellar circuit anomaly in the valproate model of autism. *Sci Rep* 9(1):9225.
36. Franks NP (2008) General anaesthesia: from molecular targets to neuronal pathways of sleep and arousal. *Nat Rev Neurosci* 9(5):370-386.
37. Rudolph U & Antkowiak B (2004) Molecular and neuronal substrates for general anaesthetics. *Nat Rev Neurosci* 5(9):709-720.
38. Alkire MT, Hudetz AG, & Tononi G (2008) Consciousness and anesthesia. *Science* 322(5903):876-880.
39. Hudetz AG, Wood JD, & Kampine JP (2003) Cholinergic reversal of isoflurane anesthesia in rats as measured by cross-approximate entropy of the electroencephalogram. *Anesthesiology* 99(5):1125-1131.
40. Tetrault S, Chever O, Sik A, & Amzica F (2008) Opening of the blood-brain barrier during isoflurane anaesthesia. *Eur J Neurosci* 28(7):1330-1341.
41. Thal SC, *et al.* (2012) Volatile anesthetics influence blood-brain barrier integrity by modulation of tight junction protein expression in traumatic brain injury. *PloS one* 7(12):e50752.
42. Fukuda M, Vazquez AL, Zong X, & Kim SG (2013) Effects of the alpha(2)-adrenergic receptor agonist dexmedetomidine on neural, vascular and BOLD fMRI responses in the somatosensory cortex. *Eur J Neurosci* 37(1):80-95.
43. Iida H, Ohata H, Iida M, Watanabe Y, & Dohi S (1998) Isoflurane and sevoflurane induce vasodilation of cerebral vessels via ATP-sensitive K+ channel activation. *Anesthesiology* 89(4):954-960.

44. Schwalm M, *et al.* (2017) Cortex-wide BOLD fMRI activity reflects locally-recorded slow oscillation-associated calcium waves. *Elife* 6.
45. Burke M, Schwindt W, Ludwig U, Hennig J, & Hoehn M (2000) Facilitation of electric forepaw stimulation-induced somatosensory activation in rats by additional acoustic stimulation: an fMRI investigation. *Magnetic resonance in medicine : official journal of the Society of Magnetic Resonance in Medicine / Society of Magnetic Resonance in Medicine* 44(2):317-321.
46. Gruters KG & Groh JM (2012) Sounds and beyond: multisensory and other non-auditory signals in the inferior colliculus. *Front Neural Circuits* 6:96.
47. Jain R & Shore S (2006) External inferior colliculus integrates trigeminal and acoustic information: unit responses to trigeminal nucleus and acoustic stimulation in the guinea pig. *Neuroscience letters* 395(1):71-75.
48. Kessler M, *et al.* (2018) Activation in the auditory pathway of the gerbil studied with (18)F-FDG PET: effects of anesthesia. *Brain Struct Funct* 223(9):4293-4305.
49. Nasrallah FA, Lee EL, & Chuang KH (2012) Optimization of flow-sensitive alternating inversion recovery (FAIR) for perfusion functional MRI of rodent brain. *NMR Biomed* 25(11):1209-1216.
50. Jenkinson M, Beckmann CF, Behrens TE, Woolrich MW, & Smith SM (2012) Fsl. *NeuroImage* 62(2):782-790.
51. Woolrich MW, Ripley BD, Brady M, & Smith SM (2001) Temporal autocorrelation in univariate linear modeling of FMRI data. *NeuroImage* 14(6):1370-1386.
52. Behzadi Y, Restom K, Liau J, & Liu TT (2007) A component based noise correction method (CompCor) for BOLD and perfusion based fMRI. *NeuroImage* 37(1):90-101.
53. Worsley KJ (2001) Statistical analysis of activation images. *Functional MRI: An Introduction to Methods*, eds Jezzard P, Matthews PM, & Smith SM (Oxford Universtiy Press, Oxford), pp 251-271.
54. Eklund A, Nichols TE, & Knutsson H (2016) Cluster failure: Why fMRI inferences for spatial extent have inflated false-positive rates. *Proceedings of the National Academy of Sciences of the United States of America* 113(28):7900-7905.
55. Friston KJ, Worsley KJ, Frackowiak RS, Mazziotta JC, & Evans AC (1994) Assessing the significance of focal activations using their spatial extent. *Human brain mapping* 1(3):210-220.
56. Smith SM & Nichols TE (2009) Threshold-free cluster enhancement: addressing problems of smoothing, threshold dependence and localisation in cluster inference. *NeuroImage* 44(1):83-98.

SUPPL REFS:

57. van der Zwaag W, *et al.* (2009) Minimization of Nyquist ghosting for echo-planar imaging at ultra-high fields based on a "negative readout gradient" strategy. *J Magn Reson Imaging* 30(5):1171-1178.
58. Paxinos G & Watson C eds (2005) *The Rat Brain in Stereotaxic Coordinates* (Elsevier Academic Press, Burlington, MA), p 209.
59. Smith SM & Brady JM (1997) SUSAN—A New Approach to Low Level Image Processing. *International Journal of Computer Vision* 23(1):45-78.
60. Jenkinson M, Bannister P, Brady M, & Smith S (2002) Improved optimization for the robust and accurate linear registration and motion correction of brain images. *NeuroImage* 17(2):825-841.
61. Smith SM (2002) Fast robust automated brain extraction. *Human brain mapping* 17(3):143-155.
62. Jenkinson M & Smith S (2001) A global optimisation method for robust affine registration of brain images. *Medical image analysis* 5(2):143-156.
63. Andersson JLR, Jenkinson M, & Smith S (2007) Non-linear optimisation. in *FMRIB technical report* (Oxford).

Supplementary Material

For the manuscript entitled:

Deciphering the scopolamine challenge rat model by preclinical functional MRI

Gergely Somogyi[1], Dávid Hlatky[1], Tamás Spisák[1, 2], Zsófia Spisák [1], Gabriella Nyitrai[1] and
András Czurkó[1]

[1] Preclinical Imaging Center, Pharmacology and Drug Safety Research, Gedeon Richter Plc., Budapest, Hungary

[2] Department of Neurology, University Hospital Essen, Essen, Germany

Supplementary Materials and Methods

Image acquisition

The MRI experiments were performed on a 9.4 T Varian (Agilent) Direct Drive MRI system (Varian Medical Systems Inc., Palo Alto, CA) with a free bore size of 210 mm, containing a 120 mm inner size gradient coil (minimum rise time 140 µs). An actively RF-decoupled quadrature-driven volume coil with an inner diameter of 72 mm (RAPID

Biomedical GmbH, Rimpar, Germany) was used for excitation, and a four-channel phased array rat brain coil (RAPID Biomedical GmbH, Rimpar, Germany) located directly above the dorsal surface of the rat's head was used for signal reception. Shimming was done to ensure a water peak linewidth of 18-26 Hz within a 5mm * 5mm * 10mm region inside the brain.

Anatomical images for the fMRI registration were proton density (PD) weighted Gradient Echo multi-slice imaging (GEMS) in the horizontal orientation, and/or a T2 weighted Fast Spin Echo multi-slice imaging (FSEMS) anatomical scans in axial orientation. (GEMS: TR / TE = 500 ms / 4.9 ms, flip angle (FA): 45°, bandwidth: 50 kHz, matrix: 256 * 256, FOV: 35 mm * 35 mm, 36 slices, slice thickness: 0.5 mm, acquisition time: 2 min 10 sec.; FSEMS: TR: 5 s, ETL: 8, effective TE: 33 ms, bandwidth: 40 kHz, matrix: 128 * 128, FOV: 22mm * 22mm, 30 axial slices, slice thickness: 1 mm, acquisition time: 1 min 20 s.)

BOLD fMRI EPI sequences

Echo Planar Imaging (EPI) sequences were used for the BOLD measurements. Gradient Echo - Echo Planar Imaging (GE-EPI: TR / TE = 1000 ms / 10 ms, FA: 90°) sequence and 1-shot Spin Echo - Echo Planar Imaging (SE-EPI: TR/TE = 1000ms/40ms, FA: 90°) sequence were used in block-design fMRI. In the case of both sequences FOV: 30 mm * 30 mm, slice thickness: 0.8 mm, 17 horizontal slices in an interleaved order, matrix: 38 * 38, resulting in isotropic spatial resolution of 8 mm. 660 images were acquired for a total acquisition time of 11 min. In Experiment 1 and Experiment 2 for both GE and SE sequences even-odd image pairs were acquired with opposite readout gradient direction and were combined for ghost removal (57) resulting in 330 images and an effective time resolution of 2 s for further analysis.

ASL fMRI sequence

For cerebral blood flow (CBF) measurements multislice arterial spin labeling with flow-sensitive alternating inversion recovery (FAIR-ASL) sequence was used as described by Nashrallah et al. (49), but the inversion bandwidth was modified to 10 kHz. Sequence summary: hyperbolic secant adiabatic inversion pulse of 20 ms and 10 kHz, followed by inversion time of 1.2 s. Multislice image acquisition was done by a single-shot SE-EPI scheme with TR/TE = 3.6 s / 18 ms, bandwidth: 250 kHz, matrix: 64 * 64, FOV: 22mm * 22mm, slice thickness: 2 mm, 9 slices were acquired in an anterior-posterior direction. A total of 50 tag-control pairs were acquired over 6 min 30 s.

Whisker stimulation

During the functional MRI experiments, the pneumatic "air-puffed" whisker stimulation was used in a block-design fashion. The stimulation was delivered to the right whisker pad of the animals through a tubing system that was integrated into the holding cradle. Air delivery timing was controlled with a magnetic valve operated by an in-house written MATLAB script (version 2009b, The MathWorks, Inc., Natick, Massachusetts, United States) via an NI USB-6215 Multifunction I/O Device (National Instruments, Austin, USA). The air pressure was set to 1 bar. Air puffs were delivered at a frequency of 1 Hz with a blowing time of 200 ms. The duration of one stimulation block was 30 s followed by 60 s rest and one measurement session, contained 6 blocks in case of the GE-EPI and SE-EPI BOLD fMRI measurements with an initial 120 s resting period after the start of imaging (660 s). In the case of the ASL-BOLD fMRI measurement, one block consisted of 36 s stimulation and a 72 s resting period. At the start of imaging, a ~60 s resting period was set. ASL measurements also contained 6 blocks: 3 consecutive blocks in two ASL measurement sessions (2 x 396 s).

Data analysis

Throughout the image processing procedure, we intended to follow the conventional human practice in fMRI analysis. Small-animal imaging specific details of the applied image processing pipeline are below described in detail.

Preprocessing

The raw images were converted to NIfTI-format (Neuroimaging Informatics Technology Initiative) by an in-house written MATLAB script (version 2009b, The MathWorks, Inc., Natick, Massachusetts, United States). The anatomical and functional images were reoriented to match the standard orientation of the digitalized version of the Rat Brain Atlas of Paxinos and Watson (58). All images were rescaled by a factor of ten to achieve image dimensions similar to human data and thus facilitate the use of image processing algorithms developed for human image analysis (34). All the approaches performed on the upscaled images were scale-invariant and does not involve any information loss. The analysis was carried out in a multistage process using the image analysis software package, FSL (50) (FMRIB's Software Library, www.fmrib.ox.ac.uk/fsl), and in-house developed software tools. FSL SUSAN (59) was used on structural images for noise reduction with nonlinear filtering to reduce noise whilst preserving the underlying structure. All the fMRI (GE, SE, and ASL) time-series were motion-corrected using MCFLIRT (60). FSL BET (Brain Extraction Tool) (61) was used to remove non-brain areas from the structural and functional images. The fractional intensity threshold was set to 0.7 and the vertical gradient in the fractional threshold was set to 0.1 for functional images. For structural images, the fractional intensity was 0.25 or 0.2 and the vertical gradient was 0.6 or 0 (based on the resolution).

To achieve spatial correspondence for the group analysis, all images were spatially standardized in two-steps (two-level registration). The functional (low-resolution) images were registered to high-resolution structural images using FSL FLIRT (62),

which utilized a 6-parameter rigid-body transformation. The high-resolution structural image was fitted to an in-house developed standard template (34) (average of 200 nonlinearly fitted structural images) by an affine transformation (FLIRT) and a nonlinear deformation field estimated by FNIRT (63). In the latter coregistration procedure, a 10 x 10 x 10 mm^3 warping field (in upscaled space) was estimated with three iterations using a relatively conservative lambda parameter set of 60, 40, and 20. This stricter regularization was applied as the morphological diversity of the rat brain is smaller compared to humans.

Functional MRI (fMRI) analysis

Gradient echo (GE) & Spin echo (SE)

Before the statistical analysis, the functional GE and SE images were spatially smoothed using a Gaussian kernel of 12.0 mm FWHM (note that the images were upscaled). High-pass temporal filtering (Gaussian-weighted least-squares straight line fitting, with sigma=162.0 s) was then applied to remove slow drifts from the signal. The fMRI data processing was carried out using FEAT (FMRI Expert Analysis Tool) Version 6.00, part of FSL. After signal prewhitening (FSL FILM), the first-level statistical analysis on the time-series was carried out using the general linear model with local autocorrelation correction (51). The analysis modeled each individual rat's data from each session and included 7 explanatory variables in total: one regressor modeling the stimuli (convolved with a double-gamma canonical HRF), its temporal derivate, to account for slight differences in timing and 5 noise-ROI-based, CompCor (52) confounder variables. For each fMRI session, a noise ROI was delineated based on the temporal signal-to-noise ratio of the BOLD signals (the upper 2 percentiles of within-brain voxels were chosen on each slice), and the first five principal components of the corresponding time-series were extracted from the data, following the broadly used t-CompCor technique.

Individual statistical Z-score images for the first regressor were obtained (average BOLD response to the stimuli). Using the spatial transformations computed during image coregistration and standardization, Z-score maps resulting from the individual statistical analysis were realigned to the common standard space to achieve spatial correspondence during the group-level analysis.

Resulting Z-score maps (both in Experiment 1 and Experiment 2) were processed in three ways for investigating the effect of individual treatment groups (saline, scopolamine, butyl-scopolamine, donepezil) and the differences between groups with a general linear model (where the factor-of-interest was the treatment). First, second-level fixed-effect statistical analysis was performed using FSL FEAT for voxelwise inference using GRF-theory-based maximum height thresholding with a (corrected) significance threshold of P=0.05 (53). This approach is robustly valid, show the mean activation in groups, but often too conservative to find differences between treatment groups because it frequently falling below 5% of family-wise error (FWE) rates (54). Similarly, for clusterwise thresholding with a corrected significance threshold of P=0.05 and cluster holding threshold of Z>3.1 was used to enhance the detection of large activation clusters unlikely to be random false positives originating from multiple comparisons (55). It gives generally better sensitivity than voxelwise inference for the disparity in the evoked responses between groups (56). Furthermore, we applied the probabilistic threshold-free cluster enhancement (pTFCE) (30) with corrected significance voxel threshold of P=0.05. In order to illustrate our results thoroughly, in some cases, we also show uncorrected pTFCE statistical inference (we thresholded our enhanced Z-score images with uncorrected $p < 0.001$ value, which corresponds to Z>3.1). This method was carried out with R software (The R Project for Statistical Computing, https://www.r-project.org) which provides a natural adjustment for various signal topologies (thereby enhanced P-values directly without permutation testing).

Arterial spin labeling (ASL)

Data processing for the ASL functional images also was carried out using FSL FEAT in order to investigate the effects of individual treatment groups (saline, scopolamine, butyl-scopolamine, donepezil) and their differences. Gaussian kernel of 12.0 mm FWHM (the images were upscaled to the human-sized brain) for spatial smoothing was used. High-pass temporal filtering (Gaussian-weighted least-squares straight-line fitting, with sigma=162 s) was then applied. After signal prewhitening, the first-level statistical analysis was carried out using the general linear model with local autocorrelation correction. The analysis modeled each individual rat's data from each session and included 11 explanatory variables in total: one regressor modeling the control-tag baseline, one for the stimuli (convolved with a double-gamma canonical HRF), and one regressor is formed by multiplying these two; their temporal derivate (3 regressors) to account for slight differences in timing; 5 noise-ROI-based, CompCor (similar to GE, SE) confounder variables.

Statistical Z-score images for the third regressor were obtained (average BOLD response to the stimuli). Using the spatial transformations (computed beforehand) Z-score maps resulting from the individual statistical analysis were realigned to the common standard. The second-level analysis utilizes the Z-score maps from the first-level evaluation and models the dependence of images by rats (due to imaging method 2 images with 3-3 blocks are generated by rats). The resulting COPE's (contrast of parameter estimates) are used in the third-level fixed-effect analysis as input data. Similar to GE, SE analysis voxelwise inference (using GRF-theory-based maximum height thresholding with a corrected significance threshold of P=0.05), clusterwise thresholding (with a corrected significance threshold of P=0.05 and cluster holding threshold of Z > 3.1), and pTFCE methods were applied.

Signal Change

The signal change is defined as the ratio of the measured signal during stimulation and resting blocks. The average of all intensities during stimulation (GE and SE: 6 * 30 s; ASL: 6* 36 s) divided by the average of all intensities during resting (GE and SE: ~120 s + 6 * 60 s; ASL: 60 s + 6 * 72 s) resulted in the signal change which is expressed in percentage (%). In our study, we show the signal change of voxels and brain areas (anatomical regions or region-of-interests – where the signal change by voxels was averaged) as well.

Relative BOLD change

The relative blood-oxygenation-level-dependent (BOLD) change is defined as the change of the signal compared to the average starting resting period (120 seconds). We have only examined this effect in the left barrel cortex in the isoflurane anesthesia (only in the gradient echo sequence) and in the combined anesthesia (GE, SE sequences as well), to investigate the effect of the whisker stimulation. After averaging the timepoints a whole-brain average and dispersion were calculated. The whole-brain average was subtracted from the voxel and it was divided by the dispersion. The relative BOLD change can show how much the anesthesia and/or the treatments affect the signal.

Supplementary Figures

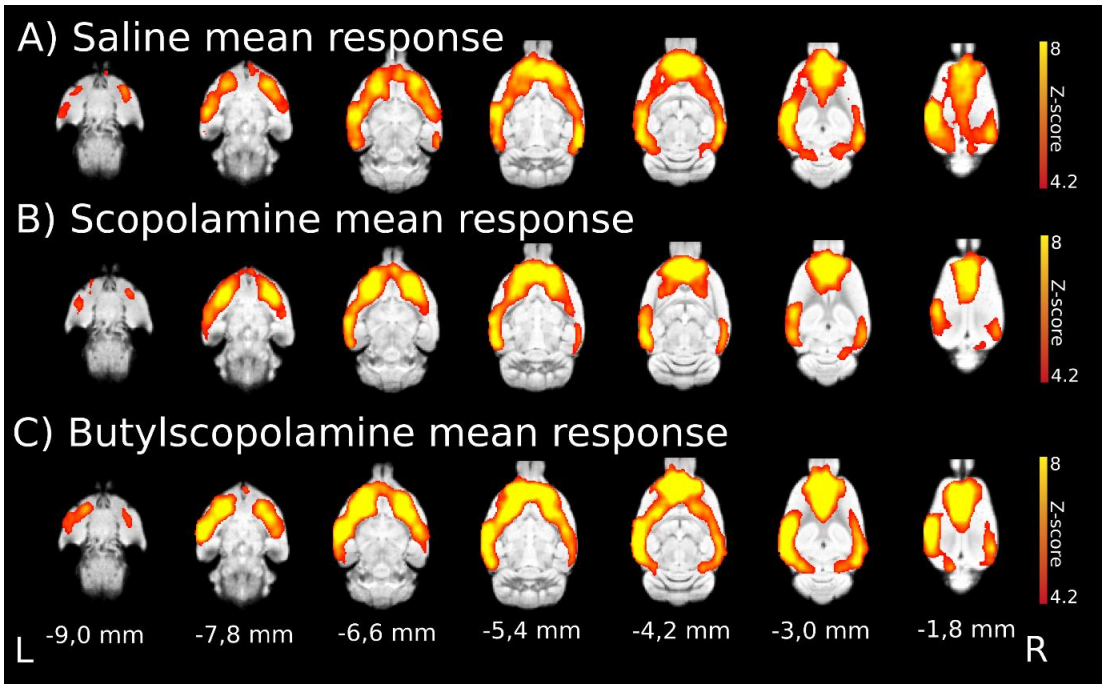

Suppl. Fig. 1. Whisker stimulation evoked gradient-echo EPI sequence BOLD responses in isoflurane anesthesia and the effect of anticholinergic modulation. *(A)* Mean activation response evoked by whisker sensory stimulation in the saline group. *(B)* Mean activation response in the scopolamine group. *(C)* Mean activation response in the butylscopolamine group. The z coordinates (distance from bregma) of the selected slices are given at the bottom of the figure (the L and R stand for the left and right directions). The Z-scores represent voxelwise ($p<0.05$, correcting for multiple comparisons via voxel significance) statistical inference (red-to-yellow from z=4.2 to z=8), the corresponding colorbars depicted on the right.

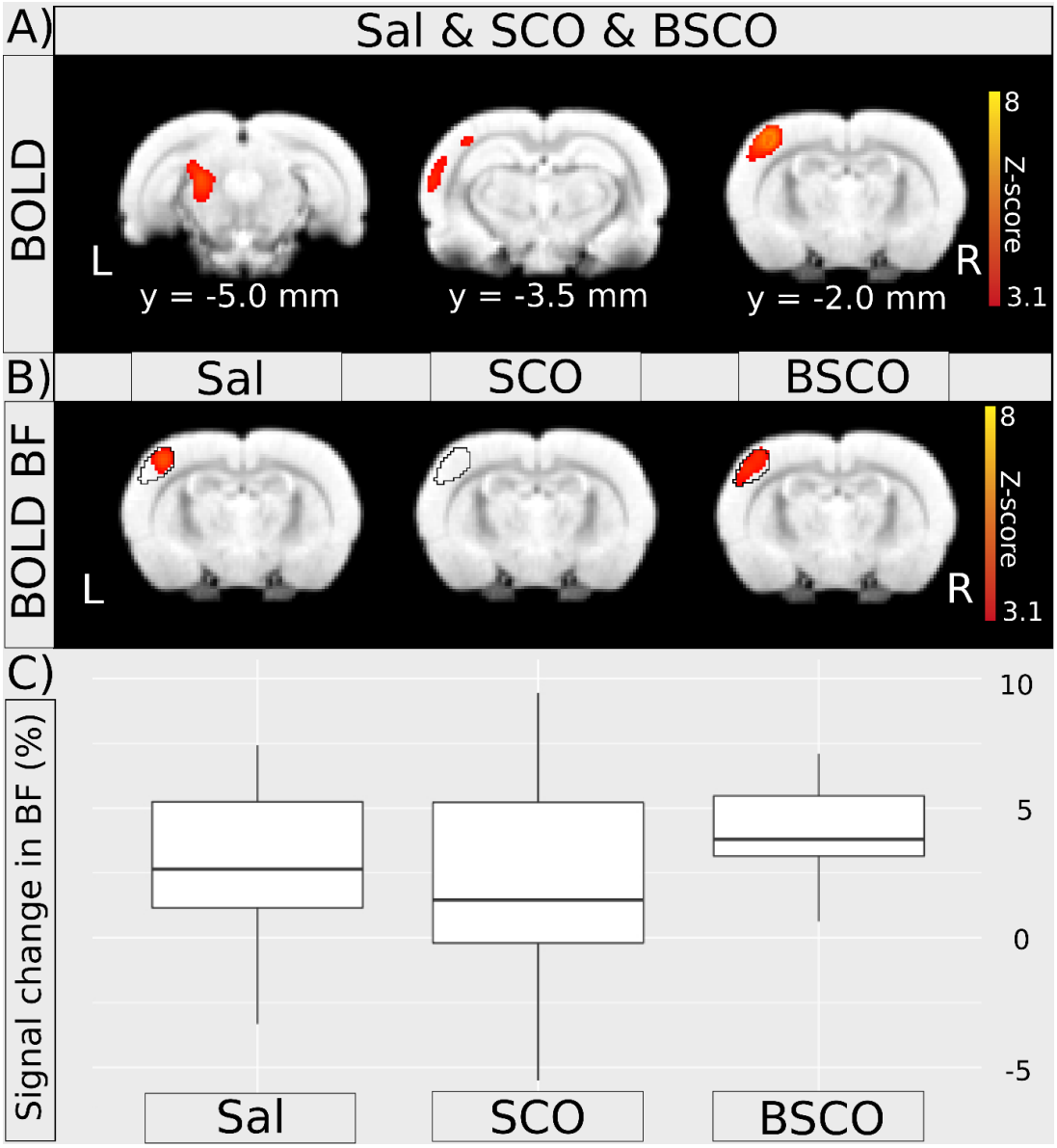

Suppl. Fig. 2. Whisker stimulation evoked arterial spin labeling (ASL) sequence BOLD responses in isoflurane anesthesia and the signal changes in the somatosensory barrel cortex (BF). *(A)* Mean BOLD activation in all treatment groups (saline, scopolamine, butylscopolamine) evoked by whisker stimulation. The y coordinates (distance from bregma) of the selected slices are given at the bottom of the figure (the L and R stand for the left and right directions). *(B)* BOLD response in the barrel field (BF) by treatment group (saline, scopolamine or butylscopolamine). The selected slices are y=-2.0 (distance from bregma). R and L stand for directions. The Z-scores represent clusterwise ($p<0.05$, correcting for multiple comparisons via cluster significance, cluster forming threshold of $z=3.1$) statistical inference (red-to-yellow

from z=3.1 to z=8), the corresponding colorbars depicted on the right. *(C)* The signal change in the BF (the region-of-interest was defined as the mean activation cluster of all treatment groups – the area is delimited by a black contour in b) by the treatment groups of the 54 ASL measurement. The difference in the means and deviations may explain that there is no significant cluster in the BF the SCO group. The scale of signal change is depicted on the right and is given in percentage (%).

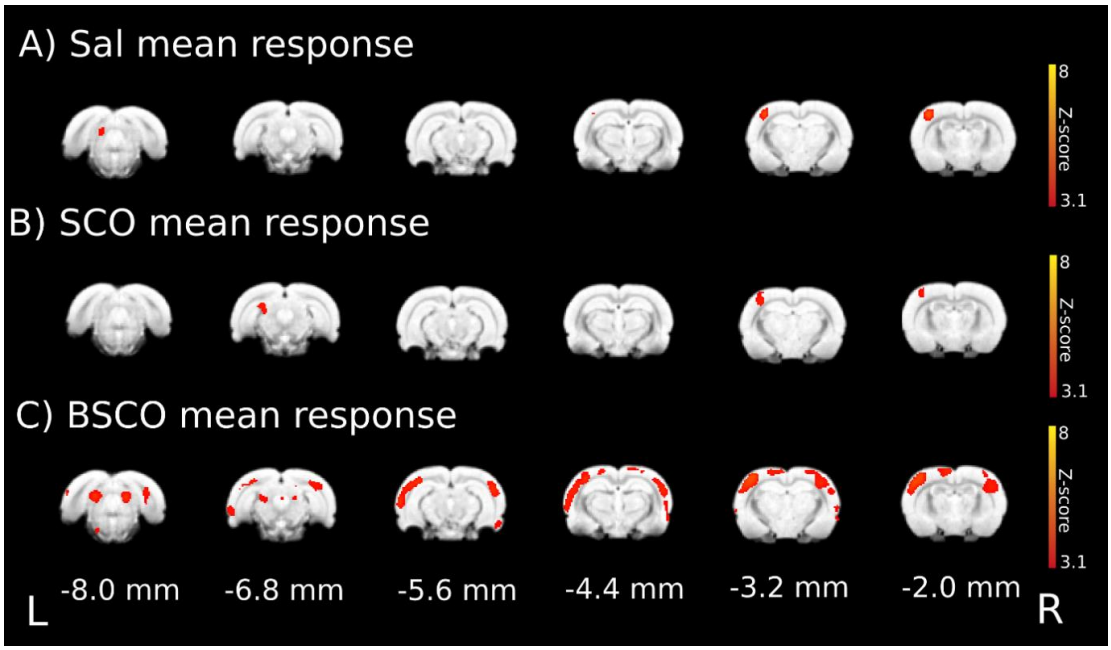

Suppl. Fig. 3. Whisker stimulation evoked functional responses with an ASL sequence in isoflurane anesthesia (uncorrected pTFCE statistics). *(A)* Mean evoked activation in the control (saline) group. *(B)* Mean evoked activation in the scopolamine group. *(C)* Mean evoked activation in the butylscopolamine group. The distance of the coronal slices from bregma (the y coordinates) are given at the bottom of the figure. Z-scores of uncorrected pTFCE statistical inference (enhanced Z-score thresholded at $p < 0.001$ value, which corresponds to $z>3.1$) depicted on the right (red-to-yellow from z=3.1 to z=8).

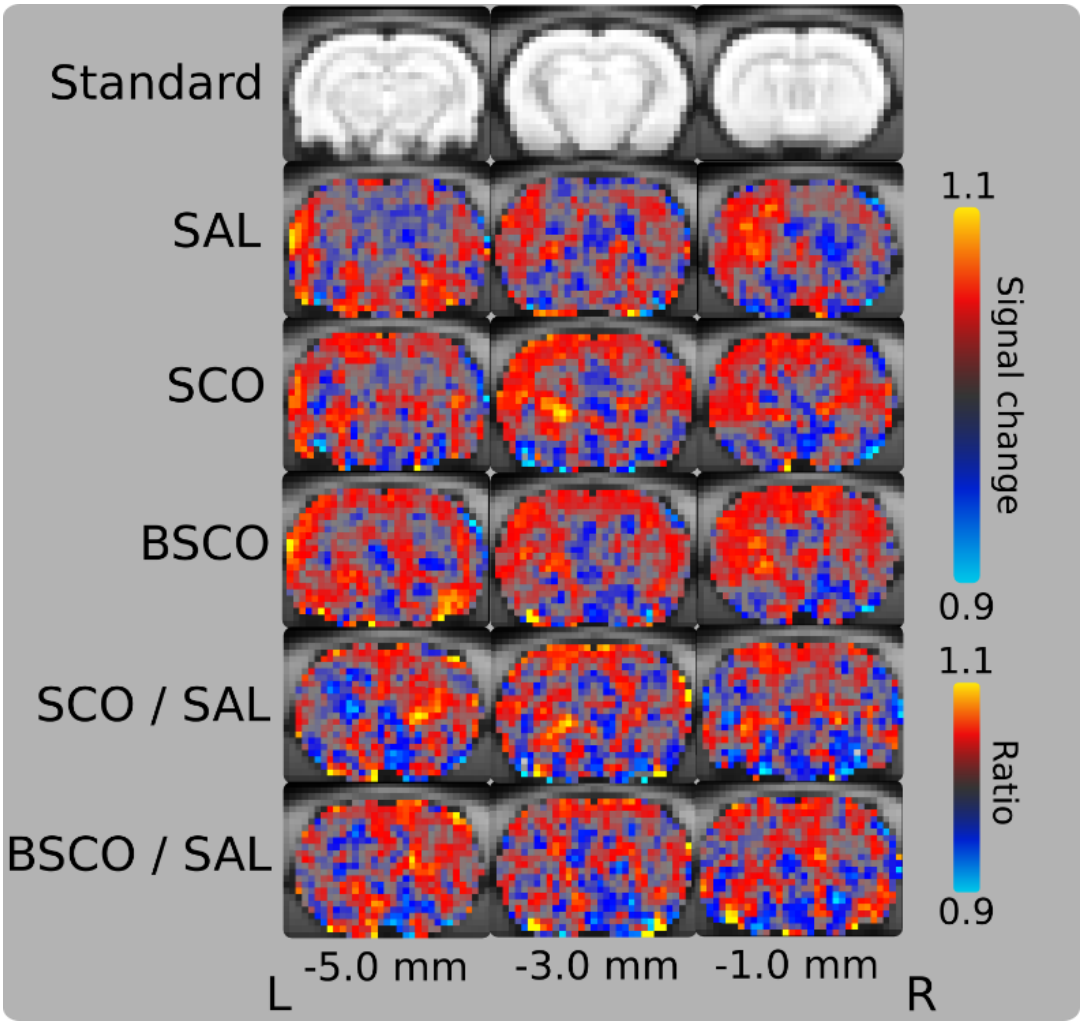

Suppl. Fig. 4. The signal change during ASL measurement in three slices. Saline, scopolamine, butylscopolamine, and the two bottom lines illustrate the ratio between scopolamine and saline, butylscopolamine and saline. The z slices distance from bregma are shown in the bottom of the figure (z = -1.0 mm, z = -3.0 mm, z = -5.0 mm; L,R stand for left and right direction). The colorbar shows the signal change or the ratio to control (typically is between 0.9 and 1.1).

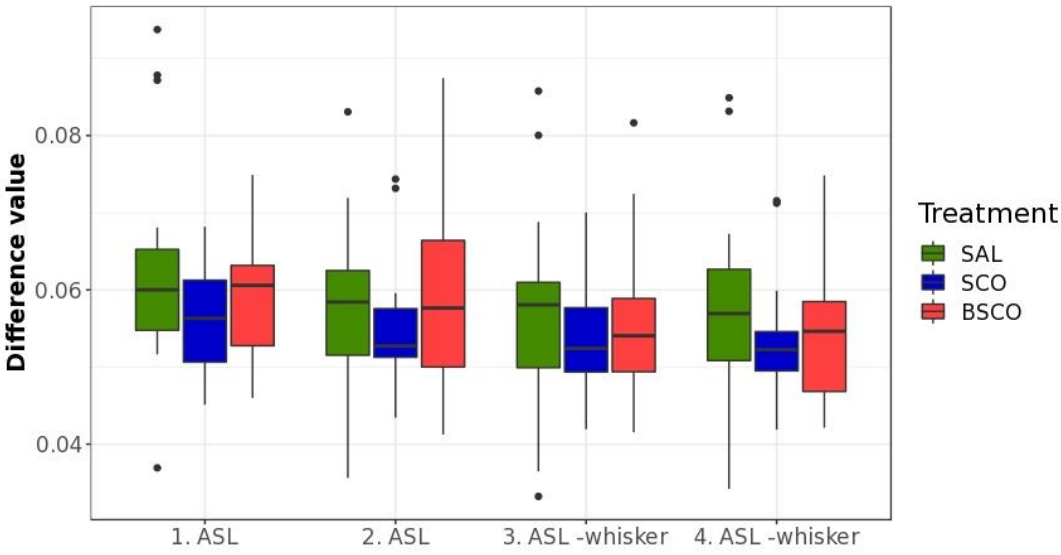

Suppl. Fig. 5. The difference between tagged and non-tagged images of every ASL measurement (in experiment 1) by treatment groups. The difference values were obtained from each voxel of ASL images: the non-tagged ones are subtracted from the tagged ones and divided by the base non-tagged. The difference values are averaged per animal and then averaged by every timepoint. The timepoints are the four different ASL measurements (two without and two with whisker stimulation). The green boxplots are the control (SAL) group, the blue ones are the SCO group and the red ones stand for BSCO. Due to this consideration, the influential effect of anesthesia (the effect of isoflurane) -the four time points are within about 25 minutes- can be excluded.

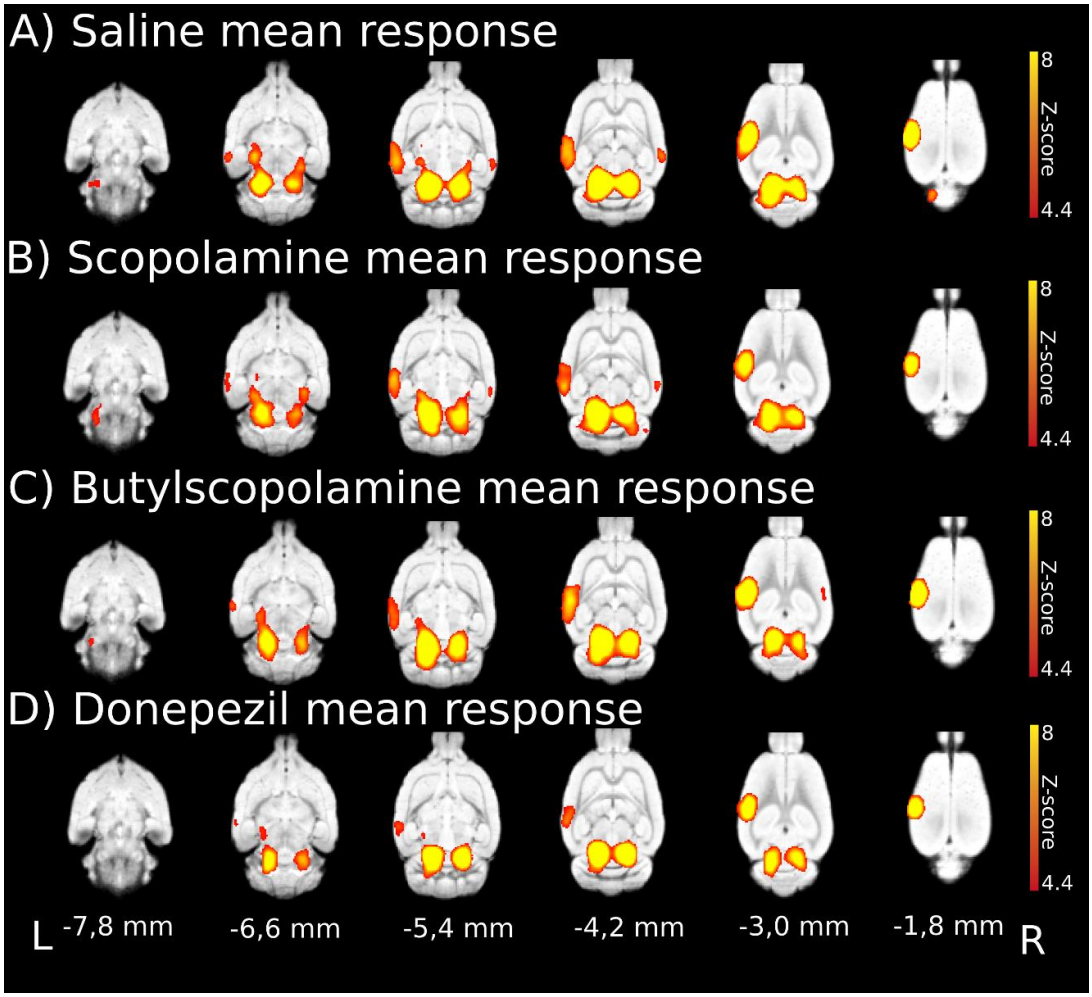

Suppl. Fig. 6. Whisker stimulation evoked gradient-echo EPI sequence BOLD responses in medetomidine-isoflurane combined anesthesia and the effect of cholinergic modulation. *(A)* Mean activation evoked by whisker sensory stimulation in control (saline) group; *(B)* mean activation in scopolamine; *(C)* in butylscopolamine and *(D)* in donepezil group with gradient-echo EPI sequence. The z coordinates (distance from bregma) and directions (left - L, right - R) are given at the bottom of the figure. Red-to-yellow Z-scores from voxelwise statistical inference ($p<0.05$, correcting for multiple comparisons via voxel significance) are shown on the right.

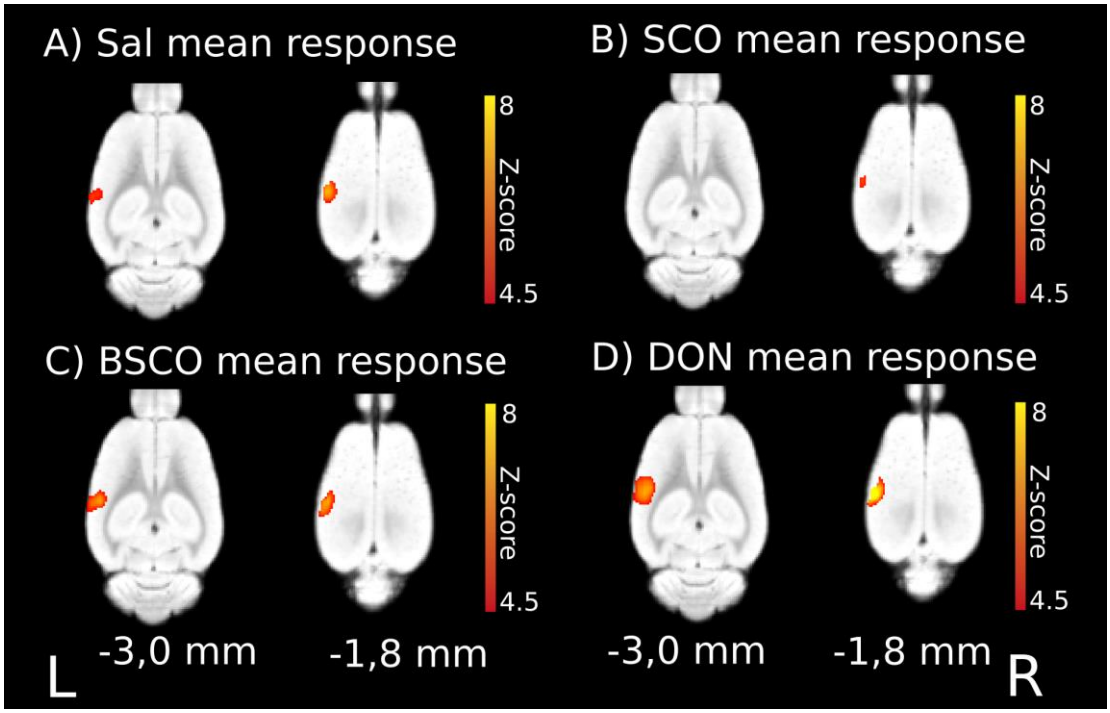

Suppl. Fig. 7. Whisker stimulation evoked spin-echo EPI sequence BOLD responses in medetomidine-isoflurane combined anesthesia. Mean activation evoked by whisker sensory stimulation in the barrel field (two slices are shown (distance from bregma): z = -3,0 mm, z = -1,8 mm). *(A)* saline, *(B)* scopolamine, *(C)* butylscopolamine and *(D)* donepezil group averages. At the bottom of the figure, the L and R stand for the left and right directions. The Z-scores represent voxelwise statistics (red-to-yellow from z=4.5 to z=8, p<0.05, correcting for multiple comparisons via voxel significance), the corresponding colorbar depicted on the right.

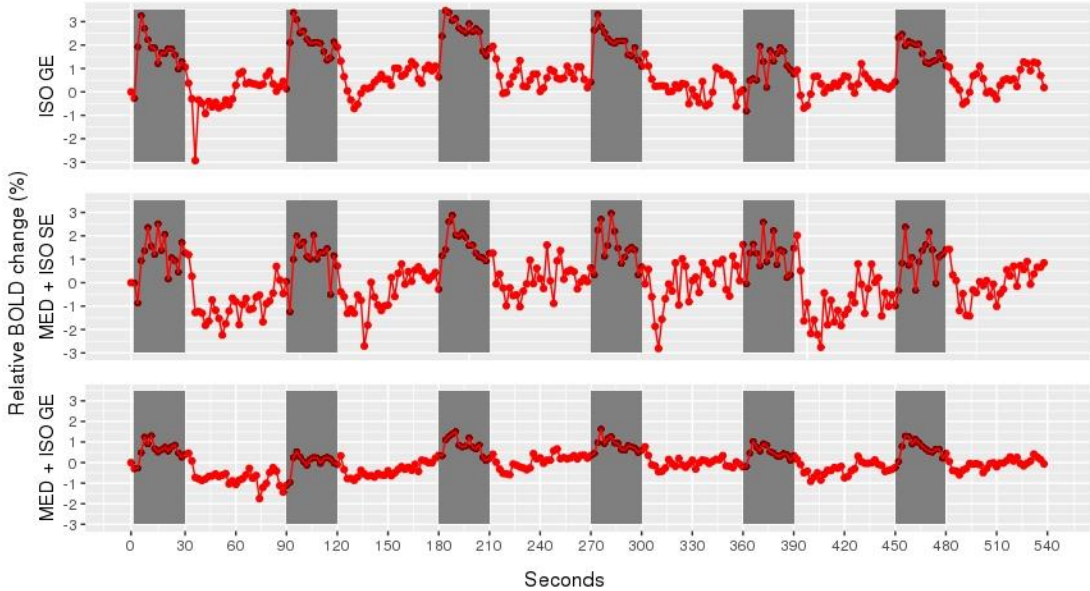

Suppl. Fig. 8. Time course of relative BOLD activation due to the six whisker stimulation blocks in the average activated barrel field (where according to the type of measurement the merged activations were Z-score > 12, voxelwise), for all EPI measurements. Top row: isoflurane (ISO) anesthesia GE sequence; middle row: combined anesthesia (MED + ISO) GE sequence; bottom row: MED + ISO anesthesia SE sequence. Every timepoint is normalized to the starting point (0. second), which is the average of the signal before the first whisker stimulation (~120 seconds). The y axis shows the relative BOLD change in percentage (%) compared to the initial resting period. The x axis shows the elapsed time in seconds. The 30 seconds long stimulation periods are darkened in the figure. The sizes of the investigated areas (where the Z-score > 12) are 10.38 mm^3; 1.56 mm^3 and 15.29 mm^3 ; in ISO GE, Med + ISO SE and Med + ISO GE, respectively.

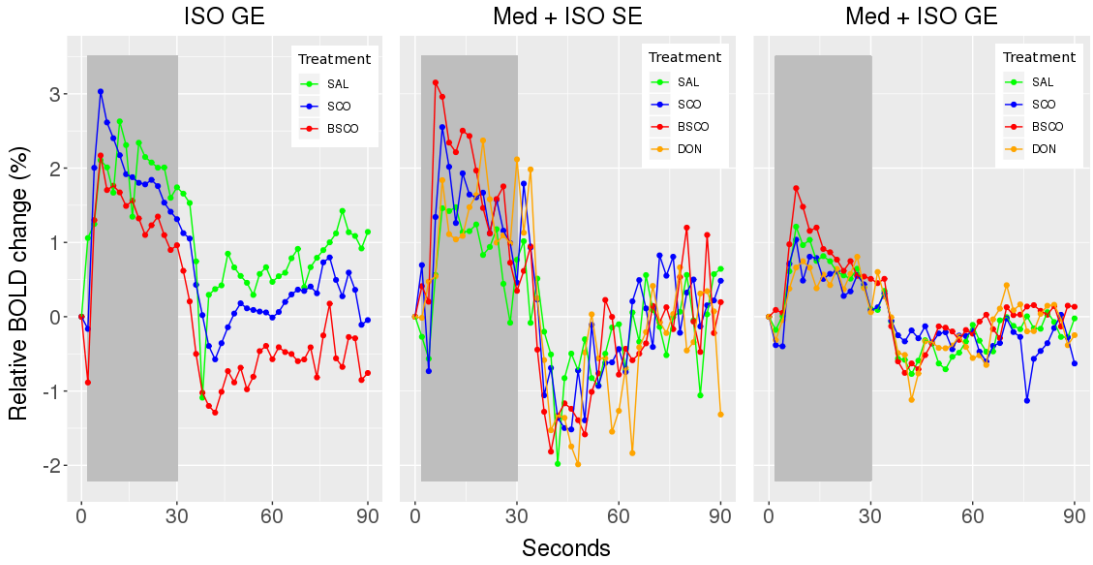

Suppl. Fig. 9. Relative BOLD change averaged into one block in the average activated barrel field (where the Z-score > 12, voxelwise). Left figure: isoflurane (ISO) anesthesia GE sequence; middle figure: combined anesthesia (MED + ISO) GE sequence; right figure: MED + ISO anesthesia SE sequence. Every timepoint is normalized to the starting point (0. second - the average of the signal before the first whisker stimulation) and averaged into one block (30 seconds on and 60 seconds off period). The y axis shows the relative BOLD change in percentage (%) compared to the initial resting period. The x axis shows the elapsed time in seconds. In each measurement, the 30-seconds-long stimulation period is darkened. The investigated areas are the same as in Fig. S9.

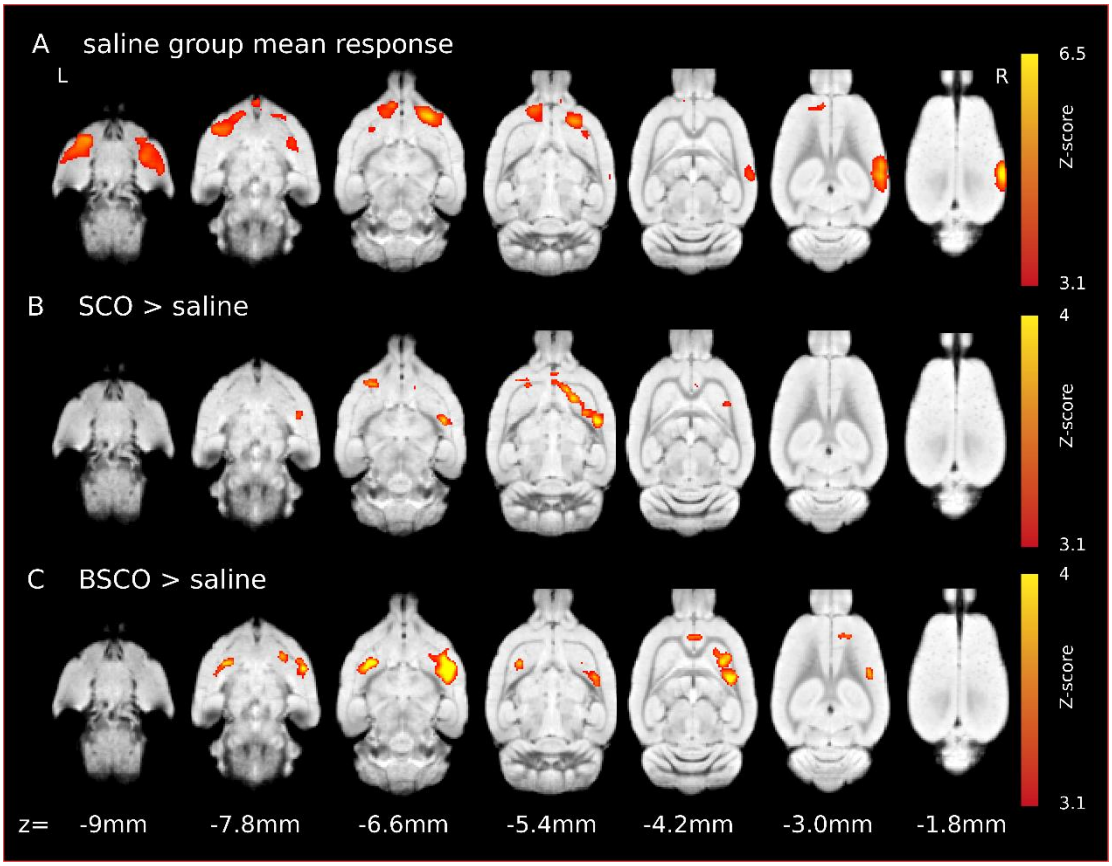

Suppl. Fig. 10. The original investigation of the effect of SCO (1 mg/kg) and BSCO (1 mg/kg) by our group: left whisker stimulation evoked gradient-echo EPI sequence BOLD responses in isoflurane anesthesia. We surprisingly observed increased BOLD activation in widespread frontal cortical areas. Mean activation evoked by whisker sensory stimulation in the barrel field ((distance from bregma): z = -9.0 mm, z = -7.8 mm, z = -6.6 mm, z = -5.4 mm, z = -4.2, z = -3.0, z = -2.6 mm). *(A)*: Sal; *(B)*: SCO > Sal and *(C)*: BSCO > Sal contrasts. The Z-scores represent clusterwise statistical inference ($p<0.05$ correcting for multiple comparisons via GRF theory based FWER and a cluster forming threshold of $p=0.01$ red-to-yellow from $z=3.1$ to $z=8$). The corresponding colorbar depicted on the right.

Supplementary Tables

Exp. 1	*Animals n =18*	*Weight at scan., (g)*	*Isoflurane dose (%)*	*Average motion (mm) GE*	*Average motion (mm) ASL*	*Respiration rate (1/min)*
Sal	*Mean (± sd)*	335.94 (± 38.48)	1.55 (± 0.11)	0.004 (± 0.002)	0.012 (± 0.003)	72.48 (± 11.60)
	Min	283	1.5	0.002	0.008	38
	Max	405	2	0.012	0.021	104
SCOP	*Mean (± sd)*	329.43 (± 34.77)	1.53 (± 0.12)	0.003 (± 0.001)	0.011 (± 0.002)	73.9 (± 11.32)
	Min	276	1	0.002	0.007	41
	Max	397	2	0.006	0.0158	103
BSCOP	*Mean (± sd)*	344.17 (± 37.07)	1.54 (± 0.13)	0.004 (± 0.002)	0.011 (± 0.003)	73.32 (± 9.52)
	Min	280	1.5	0.002	0.007	48
	Max	394	2	0.010	0.016	94

Suppl. Table 1. Summary statistics of the first experiment: weight, mean isoflurane dose, average in-scanner motion (root-mean-square (RMS) of relative displacement during GE and ASL imaging), and mean respiration rate of the rats (N=18).

Exp. 2	*Animals n = 16*	*Weight at scan., (g)*	*Isoflurane dose (%)*	*Average motion (mm) GE*	*Average motion (mm) SE*	*Respiration rate (1/min)*
Sal	*Mean (± sd)*	369.45 (± 47.94)	0.77 (± 0.30)	0.003 (± 0.001)	0.006 (± 0.001)	61.13 (±11.68)
	Min	302	0.25	0.0018	0.005	42
	Max	454	1.2	0.0044	0.011	107
SCOP	*Mean (± sd)*	367.75 (± 38.95)	0.74 (± 0.35)	0.003 (± 0.002)	0.007 (± 0.001)	64.70 (± 13.43)
	Min	288	0.1	0.002	0.005	40
	Max	433	1.5	0.008	0.009	100
BSCOP	*Mean (± sd)*	366.25 (± 28.86)	0.68 (± 0.32)	0.003 (± 0.001)	0.006 (± 0.001)	67.69 (± 12.85)
	Min	324	0.25	0.002	0.005	47
	Max	416	1.5	0.007	0.010	100
DON	*Mean (± sd)*	364.89 (± 42.98)	0.77 (± 0.33)	0.006 (± 0.003)	0.007 (± 0.002)	59.53 (± 13.26)
	Min	300	0.25	0.003	0.005	40
	Max	443	1.5	0.013	0.012	100

Suppl. Table 2. Summary statistics of the second experiment: in 0.005 mg/kg i.p. dexmedetomidine + isoflurane (0.5% - 1.5%). Weights, mean isoflurane dose, average in-scanner motion (mean RMS of relative displacement during GE and SE imaging), and mean respiration rate of the rats (N=16).

Study	*Voxelwise inference*						
	Size of blobs (mm^3)	*Z-score of local maximums (3 peaks at most per cluster)*	*Signal change (%)*	*Coordinates of local maximum*			*Structures to which local maximum Z-score belongs to:*
				x	*y*	*z*	
Exp. 1, GE	622.6	13.8	0.24	-5.1	-3.2	-2.2	L S1 BF - Left primary somatosensory cortex, barrel field
		10.8	0.16	0.3	4.8	-3.2	R PrL - Right prelimbic cortex
		10.5	0.22	0.1	3.0	-3.4	R PrL - Right prelimbic cortex
Exp. 1, ASL	0.2	4.68	4.46	-4.9	-2.2	-2.4	L S1 BF - Left primary somatosensory cortex, barrel field
Exp. 2, GE	138.6	23.7	0.60	-2.3	-9.6	-4.8	L ECIC - Left external cortex of the inferior colliculus
		15.8	0.17	1.7	-9.8	-4.4	R CIC - Right inferior colliculus
		7.78	0.12	-3.3	-6.2	-6.2	L bic –Left brachium inferior colliculus
	50.1	17.9	0.26	-5.1	-2.8	-2.2	L S1 BF - Left primary somatosensory cortex, barrel field
		7.4	1.2	-7.1	-5.4	-4.4	L Au1 - Left primary auditory cortex
		7.39	0.14	-6.9	-6	-5.6	L Au1 - Left primary auditory cortex
	3.424	6.28	0.03	6.5	-5.6	-4.2	R Au1 - Right primary auditory cortex
		5.3	0.12	6.9	-6.4	-5.4	R AuV - Right secondary auditory ventral cortex
	0.1	4.56	0.46	2.5	-13	-8.2	R Sp5I – Spinal trigeminal nucleus, interpolar
Exp. 2, SE	4.4	7.09	0.39	-5.1	-2.8	-2	L S1 BF - Left primary somatosensory cortex, barrel field

Suppl. Table 3. The size and location of the fMRI BOLD response to whisker blow in the saline group in experiment 1. (GE, ASL) and experiment 2. (GE, SE). The size of each blob, signal change (%) and the location (from Rat Brain Atlas of Paxinos and Watson) of Z-score (voxelwise statistical inference with $p<0.05$, correcting for multiple comparisons via voxel significance) local maximums (3 peaks at most per blob) of BOLD response to somatosensory stimuli in saline groups.

Exp. 1, GE							
Treat-ment	***Voxelwise***		***Clusterwise***		***pTFCE***		
	Size (mm^3)	*Structures to which maximum Z-score belongs to:*	*Size (mm^3)*	*Structures to which maximum Z-score belongs to:*	*Size (mm^3)*		*Structures to which maximum Z-score belongs to:*
					Uncor-rected (3.1 < z)	*Cor-rected (4.7 < z)*	
Sal	622.6	L S1 BF - Left primary somatosensory cortex, barrel field	853.7	L S1 BF - Left primary somatosensory cortex, barrel field	1059.8	914.6	L S1 BF - Left primary somatosenso ry cortex, barrel field
SCO	413.5	L PrL - Left prelimbic cortex	624.4	L PrL - Left prelimbic cortex	781.0	667.7	L PrL - Left prelimbic cortex
	37.4	R V1 B - Right primary visual cortex, binocular area					
BSCO	605.8	L S1 BF - Left primary somatosensory cortex, barrel field	787.0	L S1 BF - Left primary somatosensory cortex, barrel field	1000.0	841.2	L PrL - Left prelimbic cortex

Suppl. Table. 4. The size of each blob and the location (from Rat Brain Atlas of Paxinos and Watson) of Z-score maximums (Exp. 1, isoflurane anesthesia, GE) of the fMRI BOLD response to somatosensory stimuli in different treatment groups (saline, scopolamine, and butylscopolamine). Three statistical inferences (voxelwise with $p<0.05$, correcting for multiple comparisons via voxel significance; clusterwise corrected significance threshold of $p<0.05$ and cluster holding threshold of $3.1<Z$; uncorrected pTFCE-wise enhanced Z-scores thresholded at $p<0.001$, which corresponds to $3.1<Z$; corrected for multiple comparisons via voxel significance of $p<0.05$ of enhanced pTFCE Z-scores, which corresponds to $4.7<Z$) result in different cluster magnitude.

Exp. 1 GE							
Treat-ment	*Size of voxelwise blobs (mm^3)*	*Z-score local maxim um*	*Signal change (%):*	*Coordinates of local maximum*			*Structures to which Z-score maximum peak belongs to:*
				x	*y*	*z*	
Sal	622.6	13.8	0.24	-5.1	-3.2	-2.2	L S1 BF - Left primary somatosensory cortex, barrel field
		10.8	0.16	0.3	4.8	-3.2	R PrL - Right prelimbic cortex
		9.32	0.10	-6.3	-3.6	-6.6	L Au1 - Left primary auditory cortex
		9.3	-0.09	-0.1	3.0	-5.6	L IL – Left infralimbic cortex
		9.12	0.44	6.5	-7.0	-5.2	R TeA - Right temporal associatin cortex
		8.99	-0.05	3.3	2.4	-5.8	R VO - Right ventral orbital cortex
SCO	413.5	12.9	0.39	-0.1	3.6	-2.8	L PrL - Left prelimbic cortex
		10.6	0.47	-3.3	1	-6.6	L CPu – caudate putamen
		10.1	0.48	3.5	0.4	-7.4	R CPu - Right caudate putamen
		9.91	0.52	2.1	3.2	-5.0	R VO - Right ventral orbital cortex
		8.97	1.17	-6.9	-7.2	-5.0	L TeA -Left temporal associatin cortex
		8.84	0.45	-5.3	-3.4	-2.2	L S1 BF - Left primary somatosensory cortex, barrel field
	37.4	7.18	0.79	5.9	-7.4	-3.6	R V2L – Right secondary visual cortex
		5.59	-0.05	2.5	-9.8	-2.8	R prf cerebellum (near ecic)
		4.86	0.44	2.9	-5.6	-1.4	R V2ML – Right secondary visual cortex, mediolateral
BSCO	605.8	13.9	0.07	-5.5	-3.4	-2.2	L S1 BF - Left primary somatosensory cortex, barrel field
		12.4	0.03	-0.7	3.6	-4.0	L PrL - Left prelimbic cortex
		10.8	0.4	-2.7	0.4	-6.8	L CPu – Left caudate putamen
		10.7	0.09	-6.5	-3.2	-6.4	L AuV – Left secondary auditory ventral cortex
		10.6	0.22	2.3	2.6	-5.4	R VO – Right ventral orbital cortex
		10.3	0.26	-6.9	-5.6	-4.4	L Au1 - Left primary auditory cortex

Suppl. Table. 5. The size of activations of fMRI BOLD and the location (from Rat Brain Atlas of Paxinos and Watson) of voxelwise Z-score local maximums (Exp. 1, GE). The size of activation blobs in different treatment groups (Sal, SCO, BSCO), signal change (%) in local maximums, and the location (from Rat Brain Atlas of Paxinos and Watson) of the six highest Z-score are shown. The minimum peak distance is set to 3 mm.

Exp. 1, GE							
Treat-ment	*Voxelwise*		*Clusterwise*		*pTFCE*		
	Size of blobs (mm^3)	*Structures to which maximum Z-score belongs to:*	*Size of blobs (mm^3)*	*Structures to which maximum Z-score belongs to:*	*Size of blobs (mm^3)*		*Structures to which maximum Z-score belongs to:*
					Uncor-rected (3.1 < z)	*Cor-rected (4.7 < z)*	
Sal > SCO	1.5	L V1 M - Left primary visual cortex, monocular area	20.6	L V1 M - Left primary visual cortex, monocular area	251.0	56.6	L V1 M - Left primary visual cortex, monocular area
	1.2	L S1 BF - Left primary somatosensory cortex, barrel field	14.3	L S1 BF - Left primary somatosensory cortex, barrel field	15.6	-	R Ect - Right ectorhinal cortex
	0.8	L RSGc - Left retrosplenial granular cortex, c region	8.0	R S1 BF - Right primary somatosensory cortex, barrel field	0.9	-	R M1 - Right primary motor cortex
	0.2	R Ect - Right ectorhinal cortex			0.1	-	L VS - Left Ventral subiculum
					-	8.7	R S2 - Right secondary somatosensory cortex
					-	4.1	L PrS – Left presubiculum
					-	0.4	R M2 - RIght secondary motor cortex
BSCO > Sal	1.5	L Cg2 - Left cingulate cortex, area 2	9.3	L Cg2 - Left cingulate cortex, area 2	35.8	7.6	L Cg2 - Left cingulate cortex, area 2
					6.8	-	L EpP - Left epipeduncular nucleus
					0.4	-	Left agranular insular cortex, ventral part
					0.2	-	L E - Left ependymal and subependymal
					0.1	-	Ventral pallidum
BSCO > SCO	3.6	L S1 BF - Left primary somatosensory cortex, barrel field	16.5	L S1 BF - Left primary somatosensory cortex, barrel field	288.3	28.7	L S1 BF - Left primary somatosensory cortex, barrel field
	2.5	L Cg2 - Left cingulate cortex, area 2	12.5	L Cg2 - Left cingulate cortex, area 2	0.1	-	R V1 B - Right primary visual cortex, binocular area
			7.0	R S1 BF - Right primary somatosensory cortex, barrel field	-	15.8	L Cg2 - Left cingulate cortex, area 2
					-	4.0	L CPu – Left caudate putamen
					-	3.3	R S1 BF - Right primary

							somatosensory cortex, barrel field
					-	1.3	L PRh – Left perirhinal cortex
					-	0.6	R V1 B - Right primary visual cortex, monocular area
Sal > BSCO	0.5	R FrA - Right frontal association cortex			9.2	0.5	R FrA - Right frontal assocn cortex
	0.2	R FrA - Right frontal association cortex			7.4	0.1	L V1 M -Left primary visual cortex, monocular area
	0.1	L FrA -Left frontal association cortex			3	-	R PRh - Right perirhinal cortex
					2.9	-	L M2 - Left secondary motor cortex
					2.5	-	R M2 - Right secondary motor cortex
					2.4	-	R M1 - Right primary motor cortex
					2.9	-	R LO - Right lateral orbital cortex
					0.7	-	L Cl -Left Cerebellar lobes
					0.2	-	L RSD - Left retrosplenial dysgranular cortex
					-	0.1	R M2 - Right secondary motor cortex
SCO > Sal					0.2	-	L Cg1 - Left cingulate cortex, area 1
SCO> BSCO	0.4	R DLO - Right dorsolateral orbital cortex			0.8	-	R DLO - Right dorsolateral orbital cortex
	0.1	L M2 – Left secondary motor cortex			0.3	-	L M2 – Left secondary motor cortex
	0.1	L M2 - Left secondary motor cortex			0.2	-	L M2 - Left secondary motor cortex

Suppl. Table 6. The size of significant evoked BOLD activation differences between treatment groups with gradient-echo (GE) EPI sequence in isoflurane anesthesia (Exp. 1, GE). Different statistical inferences result in different cluster sizes and different cerebral structures of maximum peaks. The anatomical areas were identified using the standard orientation of the digitalized version of the Rat Brain Atlas of Paxinos and Watson.

Exp. 1, ASL								
Treatment	*Size of pTFCE-wise blobs, uncorrected Z > 3.1 (mm^3)*	*Size of pTFCE-wise blobs, corrected Z > 4.7 (mm^3)*	*Z-score of local maximum*	*Signal change (%)*	*Coordinates of local maximum*			*Structures to which local Z-score maximum belongs to:*
					x	*y*	*z*	
Sal	6.0	0.1	4.78	4.45	-4.9	-2.2	-2.4	L S1 BF - Left primary somatosensory cortex, barrel field
	1.2	-	3.62	6.40	-2.1	-8.4	-4.2	L ECIC - Left external cortex of the inferior colliculus
SCO	3.0	-	3.88	4.23	-4.5	-3.0	-2.4	L S1 BF - Left primary somatosensory cortex, barrel field
	1.0	-	3.87	7.05	-2.9	-7.2	-4.6	L bic - Left brachium of the inferior colliculus
	0.1	-	3.35	1.12	0.3	-6.4	-1.8	R RSGb - Left retrosplenial granular cortex, b region
BSCO	87.2	0.2	4.86	4.27	-4.9	-2.8	-2.0	L S1 BF - Left primary somatosensory cortex, barrel field
		-	4	10.67	-7.1	-5.2	-5	L Au1 - Left primary auditory cortex
		-	3.98	2.56	5.7	-5.6	-3.4	L V2L - Left secondary visual cortex
		-	3.96	4.95	-1.7	0.6	-1.4	L M1 - Left primary motor cortex
		-	3.94	3.20	1.7	1.8	-1.6	R M1 - Right primary motor cortex
		-	3.82	2.76	4.1	-0.8	-1.6	R S1 BF - Right primary somatosensory cortex, barrel field
	7.3	-	4.03	3.30	-2.5	-8.0	-4.4	L ECIC - Left external cortex of the inferior colliculus
	2.8	-	4.25	1.92	1.7	-7.6	-4.6	R DpWh –Right deep white layer superior colliculus
	0.5	-	3.38	5.72	-2.3	-7.8	-9.2	L VLL - Ventral nucleus of lateral lemniscus

Suppl. Table 7. The size and location of the local Z-score maximums of fMRI BOLD response to whisker blow in ASL. The size of each blob, signal change (%) and the location (from Rat Brain Atlas of Paxinos and Watson) of local maximums (pTFCE-wise enhanced uncorrected [3.1<z] and GRF corrected [p<0.05, which corresponds to 4.7<z] Z-scores) of BOLD response to somatosensory stimuli in different treatment groups. The minimum peak distance is set to 3.0 mm.

Exp. 2, GE							
Treat-ment	*Size of voxelwise blobs (mm^3)*	*Z-score local maximum*	*Signal change (%):*	*Coordinates of local maximum*			*Structures to which Z-score maximum peak belongs to:*
				x	*y*	*z*	
Sal	138.6	23.70	0.60	-2.3	-9.6	-4.8	L ECIC - Left external cortex of the inferior colliculus
		15.80	0.17	1.7	-9.8	-4.4	R CIC - Right central nu inferior colliculus
		7.78	0.18	-3.3	-6.2	-6.2	L bic –Left brachium inferior colliculus
		7.04	0.28	3.3	-7.4	-6.2	R bic – Right brachium inferior colliculus
		5.39	0.29	-3.3	-4.4	-6.4	L str – Left superior thalamic radiation
		4.82	0.35	-4.1	-10.2	-2.8	Left cerebellar lobes
	50.1	17.90	0.26	-5.1	-2.8	-2.2	L S1 BF - Left primary somatosensory cortex, barrel field
		7.40	1.21	-7.1	-5.4	-4.4	L Au1 - Left primary auditory cortex
		7.39	0.14	-6.9	-6	-5.6	L Au1 - Left primary auditory cortex
		7.31	1.22	-7.1	-4.4	-4.4	L Au1 - Left primary auditory cortex
	3.4	6.28	0.11	6.5	-5.6	-4.2	R Au1 – Right primary auditory cortex
		5.30	0.12	6.9	-6.4	-5.4	R AuV – Right secondary auditory cortex, ventral
	0.1	4.56	0.46	2.5	-13	-8.2	R Sp5I – Spinal trigeminal nucleus, interpolar
SCO	140.6	19.30	0.20	-2.3	-9.4	-5	L ECIC - Left external cortex of the inferior colliculus
		18.60	0.06	-1.9	-9.8	-4.2	L CIC - Left central nu inferior colliculus
		12.10	-0.45	1.9	-10.2	-4	Right cerebellum
		7.12	0.23	-3.1	-7.2	-6.2	L str – Left superior thalamic radiaion
		6.42	0.07	3.7	-6.6	-6.6	R PrS – Right presubiculum
	39.5	13.50	0.20	-5.1	-2.6	-2.4	L S1 BF - Left primary somatosensory cortex, barrel field
		7.38	0.56	-6.7	-5.8	-4.4	L Au1 - Left primary auditory cortex
		7.38	0.48	-7.1	-5.2	-5.8	L TeA - Left temporal associatin cortex
		6.00	0.78	-6.7	-3.4	-4.4	L Au1 - Left secondary auditory cortex, dorsal
	2.1	5.41	0.44	6.7	-6.6	-5.2	R TeA - Right temporal associatin cortex
		5.40	0.51	6.5	-6.2	-4.8	R Au1 - Right secondary auditory cortex, dorsal
		5.39	0.73	6.7	-5.6	-4.6	R Au1 - Right primary auditory cortex
	0.4	4.76	0.29	-2.9	-4.6	-7.2	L ZIC -Left zona incerta, caudal part
	0.3	4.94	-0.87	5.1	-12.2	-4.4	Right celebellar lobes
BSCO	126.8	21.1	0.14	-2.3	-9.6	-4.8	L ECIC - Left external cortex of the inferior colliculus
		12.9	-0.32	1.9	-9.8	-4.2	R ECIC - Right external cortex of the inferior colliculus
		6.77	-0.04	-3.5	-6.4	-6	L MGV -
	49.8	19.2	0.51	-5.3	-3	-2	L S1 BF - Left primary somatosensory cortex, barrel field
		6.39	0.89	-7.3	-4.6	-6	L TeA - Left temporal associatin cortex
	0.8	5.11	0.33	5.3	-2.6	-2.8	R S1 BF - Right primary somatosensory cortex, barrel field
DON	95.6	19.2	0.21	-2.1	-9.6	-4.6	L ECIC - Left external cortex of the inferior colliculus
		16	0.16	1.9	-9.8	-4.6	R ECIC - Right external cortex of the inferior colliculus

		5.77	0.34	-3.5	-6.8	-6	L MG – Left medial geniculate nucleus
		4.76	-0.23	2.5	-12.2	-7.6	Right cerebellar lobes
	29.4	14	0.06	-5.1	-2.4	-2.2	L S1 BF - Left primary somatosensory cortex, barrel field
		6.19	0.02	-6.7	-5.2	-4.4	L Au1 - Left primary auditory cortex
		6.17	0.00	-6.5	-4.6	-4.2	L Au1 - Left primary auditory cortex
		5.46	0.19	-7.1	-5.2	-5.8	L TeA - Left temporal associatin cortex

Suppl. Table 8. The size and location of the local Z-score maximums of fMRI BOLD response to whisker blow in combined anesthesia (GE). The size of each blob, signal change (%), and the location (from Rat Brain Atlas of Paxinos and Watson) of voxelwise Z-score (correcting for multiple comparisons via voxel significance of $p<0.05$) local maximums of BOLD response to somatosensory stimuli in different treatment groups. The minimum peak distance is set to 0.5 mm.

Exp. 2, GE						
Treatment	*Voxelwise*		*Clusterwise*		*pTFCE*	
	Size of blobs (mm^3)	*Structures to which maximum Z-score belongs to:*	*Size of blobs (mm^3)*	*Structures to which maximum Z-score belongs to:*	*Size of blobs (mm^3)*	*Structures to which maximum Z-score belongs to:*
Sal > SCO	3.9	L ECIC- Left external cx inferior colliculus	10.6	L ECIC- Left external cx inferior colliculus	14.2	L ECIC- Left external cx inferior colliculus
	0.1	L S1 BF- Left primary somatosensory cortex, barrel field			5.1	R ECIC- Right external cx inferior colliculus
					4.0	L S1 BF- Left primary somatosensory cortex, barrel field
					0.1	L cerebellar lobes (p.a.)
Sal > BSCO	4.1	L ECIC- Left external cx inferior colliculus	15.2	L cerebellar lobes (expanded from L ECIC)	33.6	L ECIC- Left external cx inferior colliculus
	1.3	L cerebellar lobes (p.a.)				
Sal > DON			4.0	L cerebellar lobes (expanded from L ECIC)	20.8	L cerebellar lobes (expanded from L ECIC)
SCO > Sal	0.3	L cerebellar lobes (p.a.)			4.0	L cerebellar lobes (p.a.)
					0.3	R cerebellar lobes (p.a.)
					0.2	R cerebellar lobes (p.a.)
SCO > BSCO					0.8	L cerebellar lobes (p.a.)
SCO > DON					3.1	R cerebellar lobes (p.a.) -Crus2
					0.2	L Cerebellar lobes (p.a.)
					0.1	L Vtg – Left ventral tegmental nucleus
BSCO > Sal					5.2	L Cerebellar lobes
BSCO > SCO	0.4	L S1 BF- Left primary somatosensory cortex, barrel field	4.1	L S1 BF- Left primary somatosensory cortex, barrel field	5.9	L S1 BF- Left primary somatosensory cortex, barrel field
BSCO > DON						
DON > Sal						
DON > SCO	1.2	R ECIC- Right external cx inferior colliculus	5.5	R ECIC- Right external cx inferior colliculus	6.8	R ECIC- Right external cx inferior colliculus
DON > BSCO	1.0	R cerebellar lobes (expanded from R ECIC)	4.8	R cerebellar lobes (expanded from R ECIC)	7.0	R cerebellar lobes (expanded from R ECIC)
					2.1	R cerebellar lobes (p.a.)

Suppl. Table 9. Evoked activation differences (the size of blobs in mm^3 and the structures to which Z-score peaks belong) of fMRI BOLD response to whisker blow with GE sequence between treatment groups by whisker stimuli. Rat Brain Atlas of Paxinos and Watson define the structures. Between parentheses, the abbreviation p. a. stands for presumable artifact: our gradient-echo images are not accurate enough in the cerebellum to conclude anything from these results.

Exp. 2, SE			
Treatment	*Size of voxelwise blobs (mm^3)*	*Structures to which voxelwise Z-score peak belongs to:*	*Average signal increase in the related structures (%):*
Sal	4.4	L S1 BF - Left primary somatosensory cortex, barrel field	0.38
SCO	1.3	L S1 BF - Left primary somatosensory cortex, barrel field	0.50
BSCO	6.3	L S1 BF - Left primary somatosensory cortex, barrel field	0.15
DON	8.4	L S1 BF - Left primary somatosensory cortex, barrel field	0.02

Suppl. Table 10. The size (mm^3) and location of the evoked mean BOLD response in saline, scopolamine, butylscopolamine, and donepezil groups with SE sequence in isoflurane-medetomidine combined anesthesia. Rat Brain Atlas of Paxinos and Watson define structures to which voxelwise Z-score (correcting for multiple comparisons via voxel significance of $p<0.05$) peaks belong to. Signal change in the structure is defined as the ratio of the average signal during the whisker stimulation and resting periods.

Andersson, J. L. R., Jenkinson, M., & Smith, S. (2007). *Non-linear optimisation.* Retrieved from Oxford:

Behzadi, Y., Restom, K., Liau, J., & Liu, T. T. (2007). A component based noise correction method (CompCor) for BOLD and perfusion based fMRI. *Neuroimage, 37*(1), 90-101. doi:10.1016/j.neuroimage.2007.04.042

Eklund, A., Nichols, T. E., & Knutsson, H. (2016). Cluster failure: Why fMRI inferences for spatial extent have inflated false-positive rates. *Proc Natl Acad Sci U S A, 113*(28), 7900-7905. doi:10.1073/pnas.1602413113

Friston, K. J., Worsley, K. J., Frackowiak, R. S., Mazziotta, J. C., & Evans, A. C. (1994). Assessing the significance of focal activations using their spatial extent. *Hum Brain Mapp, 1*(3), 210-220. doi:10.1002/hbm.460010306

Jenkinson, M., Bannister, P., Brady, M., & Smith, S. (2002). Improved optimization for the robust and accurate linear registration and motion correction of brain images. *Neuroimage, 17*(2), 825-841.

Jenkinson, M., Beckmann, C. F., Behrens, T. E., Woolrich, M. W., & Smith, S. M. (2012). Fsl. *Neuroimage, 62*(2), 782-790. doi:10.1016/j.neuroimage.2011.09.015

Jenkinson, M., & Smith, S. (2001). A global optimisation method for robust affine registration of brain images. *Med Image Anal, 5*(2), 143-156.

Nasrallah, F. A., Lee, E. L., & Chuang, K. H. (2012). Optimization of flow-sensitive alternating inversion recovery (FAIR) for perfusion functional MRI of rodent brain. *NMR Biomed, 25*(11), 1209-1216. doi:10.1002/nbm.2790

Paxinos, G., & Watson, C. (Eds.). (2005). *The Rat Brain in Stereotaxic Coordinates*. Burlington, MA: Elsevier Academic Press.

Smith, S. M. (2002). Fast robust automated brain extraction. *Hum Brain Mapp, 17*(3), 143-155. doi:10.1002/hbm.10062

Smith, S. M., & Brady, J. M. (1997). SUSAN—A New Approach to Low Level Image Processing. *International Journal of Computer Vision, 23*(1), 45-78. doi:10.1023/a:1007963824710

Smith, S. M., & Nichols, T. E. (2009). Threshold-free cluster enhancement: addressing problems of smoothing, threshold dependence and localisation in cluster inference. *Neuroimage, 44*(1), 83-98. doi:10.1016/j.neuroimage.2008.03.061

Spisak, T., Pozsgay, Z., Aranyi, C., David, S., Kocsis, P., Nyitrai, G., . . . Kincses, Z. T. (2017). Central sensitization-related changes of effective and functional connectivity in the rat inflammatory trigeminal pain model. *Neuroscience, 344*, 133-147. doi:10.1016/j.neuroscience.2016.12.018

Spisak, T., Spisak, Z., Zunhammer, M., Bingel, U., Smith, S., Nichols, T., & Kincses, T. (2018). Probabilistic TFCE: A generalized combination of cluster size and voxel intensity to increase statistical power. *Neuroimage, 185*, 12-26. doi:10.1016/j.neuroimage.2018.09.078

van der Zwaag, W., Marques, J. P., Lei, H., Just, N., Kober, T., & Gruetter, R. (2009). Minimization of Nyquist ghosting for echo-planar imaging at ultra-high fields based on a "negative readout gradient" strategy. *J Magn Reson Imaging, 30*(5), 1171-1178. doi:10.1002/jmri.21951

Woolrich, M. W., Ripley, B. D., Brady, M., & Smith, S. M. (2001). Temporal autocorrelation in univariate linear modeling of FMRI data. *Neuroimage, 14*(6), 1370-1386. doi:10.1006/nimg.2001.0931

Worsley, K. J. (2001). Statistical analysis of activation images. In P. Jezzard, P. M. Matthews, & S. M. Smith (Eds.), *Functional MRI: An Introduction to Methods* (pp. 251-271). Oxford: Oxford Universtiy Press.